Photometric Recovery of Crowded Stellar Fields Observed with *HST*/WFPC2 and the Effects of Confusion Noise on the Extragalactic Distance Scale

Laura Ferrarese
University of California Los Angeles, CA, 90095, USA, laura@astro.ucla.edu

N.A. Silbermann
Infrared Processing and Analysis Center, Caltech, Pasadena CA 91125, USA, nancys@ipac.caltech.edu

Jeremy R. Mould
Research School of Astronomy & Astrophysics, Institute of Advanced Studies, ANU, ACT 2611, Australia, jrm@mso.anu.edu.au

Peter B. Stetson
Dominion Astrophysical Observatory, Victoria, British Columbia V8X 4M6, Canada, Peter.Stetson@hia.nrc.ca

Abhijit Saha
Kitt Peak National Observatory, NOAO, Tucson AZ 85726, USA, saha@noao.edu

Wendy L. Freedman
Observatories of the Carnegie Institution of Washington, Pasadena, CA 91101, USA, wendy@ociw.edu

Robert C. Kennicutt, Jr.
Steward Observatory, University of Arizona, Tucson, AZ 85721, USA, robk@as.arizona.edu

To appear in the February 2000 issue of the PASP

ABSTRACT

We explore the limits of photometric reductions of crowded stellar fields observed with the Wide Field and Planetary Camera 2 on board the *Hubble Space Telescope*. Two photometric procedures, based on the DoPHOT and DAOPHOT/ALLFRAME programs are tested, and the effects of crowding, complex sky background and cosmic-ray (CR) contamination are discussed using an extensive set of artificial star simulations. As a specific application of the

results presented in this paper, we assess the magnitude of photometric biases on programs aimed at finding Cepheids and determining distances. We find that while the photometry in individual images can be biased too bright by up to 0.2 mag in the most crowded fields due to confusion noise, the effects on distance measurements based on Cepheid variables are insignificant, less than 0.02 mag (1% in distance) even in the most problematic cases. This result, which is at odds with claims recently surfaced in the literature, is due to the strict criteria applied in the selection of the variable stars, and the photometric cross checks made possible by the availability of multiple exposures in different filters which characterizes Cepheid observations.

Subject headings: cosmology: distance scale — galaxies: photometry — galaxies: distance and redshifts — techniques: photometric

1. INTRODUCTION

During its six years of operation, the Wide Field and Planetary Camera 2 (WFPC2) on board the *Hubble Space Telescope* (*HST*) has produced several thousand hours' worth of observations of crowded stellar fields, from Galactic globular clusters to distant galaxies. The photometric reduction of such fields is challenging. Much effort has been spent in calibrating the photometric zero points and assessing the magnitude of non-linearity effects (Holtzmann et al. 1995, Whitmore & Hayer 1997, Hill et al. 1998, Stetson 1998, Saha et al. 2000), but not enough attention has been devoted to understanding whether and to what extent biases are introduced by the procedures used for the photometric analysis. Recently, Mochejska et al. (1999) and Stanek & Udalski (1999) addressed the effects of confusion noise on distance measurements based on Cepheid variable stars, and concluded that for galaxies at 20 Mpc observed with *HST*, distances are underestimated by up to 15% due to blending. These studies are based on a simple extrapolation to large distances of ground-based Cepheid observations in M31 and LMC fields. Unfortunately, they make two invalid assumptions: that the photometric reduction procedures are incapable of recognizing and correcting for the increasing level of crowding at larger distances, and that the stellar background in the M31 and LMC fields are representative of those of the more distant galaxies. A more direct assessment of the effects of crowding on the DoPHOT (Schechter et al. 1993) photometry of one particular galaxy, NGC 4639, which was targeted for Cepheids by Saha et al. (1997) using *HST*, is presented by Saha et al. (2000). For this galaxy, which is at a distance of ~ 25 Mpc, the authors find a 5% bias in distance due to crowding, much smaller than inferred by Mochejska et al. and Stanek & Udalski, but still significant.

In this paper we test both DoPHOT and DAOPHOT/ALLFRAME (ALLFRAME from now on for simplicity, Stetson 1994) photometric procedures using an extensive set of artificial star simulations of fields spanning a wide range of crowding and complexity of the underlying background. The analysis presented in this paper has specific applications to the results of the '*HST* Key Project on the Extragalactic Distance Scale' (hereafter Key Project, Kennicutt, Freedman, & Mould 1995), and the 'Type Ia Supernovae Calibration Project' (e.g., Sandage et al. 1992), but is also relevant to any DoPHOT and ALLFRAME photometric reduction of crowded stellar fields observed with the WFPC2.

The construction of the artificial star frames is discussed in §2, and the procedure used in the photometric analysis in §3. The results are presented in §4, §5 and §6. Section 4 describes control tests done on uncrowded, constant background artificial star fields, while §6 deals with the effects of confusion noise for both DoPHOT and ALLFRAME. DoPHOT has also been subjected to two additional test: Section 5 dissects the effects of CRs on the DoPHOT photometry of crowded fields, and a simple test of the accuracy of the DoPHOT photometric calibration is given in §7. These tests were done for DoPHOT and not ALLFRAME without implying that we expect the former to be more affected; similar tests could also be carried out for ALLFRAME. Finally, §8 presents a summary of results.

2. CONSTRUCTION OF THE ARTIFICIAL STAR FRAMES

Of the fields targeted by the Key Project we selected two at opposite extremes in terms of complexity of the background, confusion from crowding and incidence of CR hits: the nearby galaxy NGC 2541 (d$\sim$12 Mpc) and NGC 1365 in the Fornax cluster (d$\sim$19 Mpc). Most of the galaxies observed by the Key Project fall in between these two extremes in terms of sky brightness and crowding, both across the field and specifically in the regions where Cepheids are found, with very few galaxies approaching the level of complexity presented by the NGC 1365 field. Montages of the four WFPC2 CCDs for each field (from which CRs have been removed) are shown in Figures 1 and 2. For each galaxy, four out of the twelve existing epochs of observations were selected, each with pairs of back to back exposures (referred to as a 'CR-split pairs') in both the F555W and F814W filters. Exposure times and other relevant information are given in Table 1.

The artificial stars used to test both DoPHOT and ALLFRAME are created using exclusively ALLFRAME parameters, in particular: 1) the average PSFs constructed for the ALLFRAME analysis are assumed to be faithful reproductions of the true system PSFs; and 2) the ALLFRAME photometric calibration is used to transform the instrumental PSF magnitudes to F555W and F814W magnitudes in the Holtzmann et al. (1995) ground

based system (see §3). In the ALLFRAME procedure followed by the KP, the PSF is constructed from WFPC2 images of uncrowded stellar fields, and is then used for the ALLFRAME photometric analysis of *all* of the observed galaxies. However, the WFPC2 PSF changes with time due, for example, to focus changes and telescope jitter: these will lead to systematic variations in the profile-fitting magnitudes in frames that have true PSFs very different from the mean PSFs. In the ALLFRAME reduction stream, magnitude corrections are determined by measuring a number of hand-selected local standards in each field through a series of synthetic apertures up to one-half arcsecond in radius. These aperture magnitudes, projected to a fixed aperture radius of one-half arcsecond through a growth-curve analysis (Stetson 1990) are presumed to be insensitive to focus and tracking errors; the mean difference between these aperture magnitudes and the profile-fitting magnitudes for a given frame are applied to the latter as an 'aperture correction'.

DoPHOT takes the opposite approach: for each photometered frame, the PSF is determined within the frame using suitable bright and isolated stars throughout the field, so while different frames will generally have different PSFs, the aperture corrections are maintained relatively constant. Adding stars described by the ALLFRAME PSFs to an existing galaxy frame has the inevitable consequence that the artificial stars added to the images will by definition have the fiducial PSFs and will not be subject to the same aperture corrections as the actual stars in those same images. Therefore, the artificial star experiments described here are not effective in testing the validity of the aperture corrections or photometric zero points for either reduction procedures: by definition, the artificial star magnitudes recovered by ALLFRAME will agree *in the mean* with the input magnitudes, while the errors in both the DoPHOT and ALLFRAME aperture corrections will limit the significance of any difference between the input and DoPHOT recovered magnitudes. Adopting an ALLFRAME PSF for the artificial stars does not, however, affect our ability to study crowding-induced photometric scatter and scale errors.

Two thousand artificial stars with given right ascension, declination and V and I magnitudes were generated using the ALLFRAME PSF and the luminosity functions shown by the solid black lines in Figures 3 and 4. Figures 1 and 2 show images of the artificial star frames. Poisson noise was added to the artificial stars, however no read noise or Poisson noise was added to the sky since these noise sources are already present in the real galaxy frames. No artificial stars were placed close to the edges of the chips, which are vignetted by the pyramid mirror. The artificial stars were then added to each of the NGC 2541 and NGC 1365 frames listed in Table 1.

2.1. Nomenclature

In what follows we will refer to the frames containing only the artificial stars on a zero background as the 'artificial frames', to the original galaxy frames as the 'real frames' and to the original galaxy frames to which the artificial stars have been added as the 'real+artificial frames'. We will speak of an 'exposure' in reference to a single image of a CR-split pair (for example U2S72901T, see Table 1), and of an 'epoch' in reference to the image obtained by combining two CR-split exposures (for example U2S72901T and U2S72902T, see §3.1). 'Input magnitudes' are the ones assumed in constructing the artificial star frames, by definition they do not have an associated error. 'Recovered magnitudes' are the ones measured by running ALLFRAME or DoPHOT on the frames; they will differ from the input magnitudes due to the modeled photon statistics, the underlying read noise and sky noise in the real frames, and the effects of crowding.

3. PHOTOMETRIC PROCEDURE: APPLICATION OF ALLFRAME AND DoPHOT

The real+artificial frames and the artificial frames were photometered by NAS using ALLFRAME (Stetson 1994) and by LF using a variant of DoPHOT especially formulated to deal with the undersampling of WFPC2 data (Schechter, Mateo, & Saha 1993; Saha et al. 1994). Neither NAS nor LF had access to the artificial star list (created by PBS) until after the photometric analysis was complete. We followed the methodology of the Key Project (e.g., Hill et al. 1998, Ferrarese et al. 1996), except that only a subset of eight of the 24 Key Project exposures of each field (four of 12 epochs), were used to derive the master star list. As usual, all images are multiplied by four and converted to integer before the photometric analysis is performed. Therefore, the effective gain is 1.75 e^-, as opposed to 7 e^- of real WFPC2 data.

3.1. DoPHOT Photometric Reduction

Each pair of back to back CR-split exposures was combined – to obtain what we will be referring to as an 'epoch frame'– and CRs were removed prior to the DoPHOT run. Further details of the DoPHOT procedure can be found in Ferrarese et al. (1998) and Saha et al. (1994). Table 2 lists the PSF parameters (FWHM along the major and minor axes and tilt angle) reported by DoPHOT for the real frames, the artificial star frames, and the real+artificial frames. The artificial stars' luminosity function is more heavily weighted

towards bright magnitudes, so while the PSF fitted by DoPHOT to the real frames is slightly different from the artificial star PSF, the PSF fitted to the real+artificial star frames is very close.

The DoPHOT aperture corrections needed to transform the fitted magnitudes to the $0''.5$ magnitudes defined by Holtzmann et al. (1995) were calculated independently for each photometered frame, following Ferrarese et al. (1998). Some of the DoPHOT aperture corrections are listed in Table 3 for the artificial star frames, and for the first exposure and first epoch (the two exposures of the first CR-split pair combined, see Table 1) of the real+artificial star frames. The number of stars used in deriving the aperture corrections is shown in parentheses in each case. Because of jitter and focus changes, aperture corrections for other exposures/epochs differ from those of the first epoch and from each other by up to 0.05 mag. For comparison, the aperture corrections derived for an uncrowded field in Leo I are also shown. Notice that because the DoPHOT aperture corrections are derived from a mixture of real and artificial stars, which (for DoPHOT) are not described by an identical PSF, the DoPHOT aperture corrections might not be appropriate for either real or artificial stars, and any zero point comparison quoted in this paper is of very limited significance.

Finally, the aperture corrected magnitudes were transformed to the F555W and F814W magnitudes on the Holtzmann et al. ground based system following Hill et al. (1998); the final transformation to V and I magnitudes, which requires the addition of a V–I color term (the same for DoPHOT and ALLFRAME, and up to 0.02 mag for F555W and 0.04 mag for F814W), is not necessary for our purpose.

3.2. DAOPHOT/ALLFRAME Photometric Reduction

As customary, ALLFRAME was run on all eight exposures simultaneously. Notice that for a typical galaxy observed by the KP, ALLFRAME would be run simultaneously on a larger sample of ~ 30 frames, therefore in the case discussed here ALLFRAME has a less than typical ability to recognize blended images. The ALLFRAME fitted PSF is, of course, identical to the artificial PSF by construction. The aperture corrections for the first and second exposures are as given in Table 4, notice that these are more recent than the ones used by Ferrarese et al. (1998) and Silbermann et al. (1999) for the original reduction of the galaxy frames. As for the DoPHOT procedure, the aperture corrected magnitudes are transformed to F555W and F814W magnitudes following Hill et al. (1998).

4. CONTROL TESTS ON THE ARTIFICIAL FRAMES

A control experiment was done by running DoPHOT and ALLFRAME on the uncrowded, zero background, CR-free artificial star frames constructed for NGC 1365 (the NGC 2541 artificial frames will not be discussed as they do not differ from the NGC 1365 frames in any relevant way). The luminosity function of the recovered stars is shown in Figure 3 by the thick red and green lines for ALLFRAME and DoPHOT. Only the PC and WF2 chips are shown as the results for the other two chips are comparable. Notice that at faint magnitudes DoPHOT is more complete than ALLFRAME in both chips, *a posteriori* we attribute this result to a more sensitive detection threshold (the number of sigma above the background needed to trigger a detection) adopted in the DoPHOT run. Figures 5 and 6 show a comparison of input magnitudes and the magnitudes recovered by ALLFRAME and DoPHOT for the PC and WF2 (the results for the other chips are similar). A weighted mean and standard deviation σ (where the weights are given by the inverse of the DoPHOT reported errors) of the difference Δm between input and recovered magnitudes is calculated by excluding all points deviating by more than 2σ from the mean, and iterating the process until convergence. This typically excludes 25% of the stars in F555W and 35% in F814W. Stars fainter than 28 mag are also excluded. The results are listed in Table 5, where we also report the slope $\gamma = [\Delta m/\text{input mag}]$ and standard deviation derived from a least-squares fit to all data points. A non-zero γ would indicate the presence of non-linearities in the photometry: for example, if the sky were systematically overestimated, fainter stars would be affected more than bright ones, and γ would be negative. As expected, both DoPHOT and ALLFRAME perform well on these simple frames. No non-linearity effects are seen. Notice that the perfect agreement in magnitude between input and recovered magnitudes for ALLFRAME is artificial and results from having adopted the ALLFRAME photometric calibration for the artificial stars. In view of the fact that ALLFRAME aperture corrections for NGC 1365 are based only on a handful of stars (Table 4), and the differences between the ALLFRAME and DoPHOT PSFs, especially for the PC (Table 2), the agreement between input and recovered magnitudes for DoPHOT is also good. The solid flaring curves in Figures 5 and 6 represent the typical error reported by DoPHOT and ALLFRAME for stars at any given magnitude. The percentage of stars with difference between input and measured magnitude larger than three times the reported σ is about 0.6% for DoPHOT and 0.7% for ALLFRAME, which confirms the reliability of the error estimates as given by both photometric procedures.

5. EFFECTS OF COSMIC RAY HITS: DoPHOT TESTS

ALLFRAME and DoPHOT take very different approaches when dealing with CR hits. Because ALLFRAME runs simultaneously on all available exposures, information on the position and magnitudes of each object is carried from frame to frame and CRs are easily flagged. DoPHOT identifies CRs as differing significantly from a stellar PSF. Objects in each frame are identified with the help of a master star list created from a deep, CR-free image obtained by combining all exposures. DoPHOT parameters can be set so that objects identified in a single exposure but not present in the master star list will be classified as CRs unless their PSF is virtually identical to a stellar PSF. This flags the majority of CR hits, but DoPHOT can still err when CRs hit the centers of stars included the master star list. For this reason, DoPHOT is more reliable when applied to frames from which CRs have been removed. This is an easy task for the Key Project galaxies since, with very few exceptions, CR-split pairs are available for each epoch. The CR-split exposures are combined before processing with DoPHOT and CRs are identified when the difference in counts between corresponding pixels (after accounting for a global difference in the sky level) is larger than four times a local sigma calculated from the combined effects of Poisson statistics and local noise.

This procedure poses some questions. Because of the severe undersampling of the WFPC2, particular care must be taken to assure that the peaks of bright stars are not erroneously identified as CR hits while combining the CR-split pairs. In addition, unidentified CR events could lead to an overestimate or an underestimate of the stellar magnitudes, depending on whether the hits fall on top of a stellar PSF or in the nearby region used to measure the sky respectively. We have conducted the following test to assess the effects of CR events on the DoPHOT photometry. For the real+artificial star frames of both NGC 2541 and NGC 1365 we ran DoPHOT independently on the first and second exposure of the first epoch for each galaxy, which are heavily affected by CRs, and on the CR-cleaned first epoch frame, produced by combining the first and second exposure. In all cases the master star list derived from all exposures combined was used. Figure 7 shows a comparison of sky values measured in the first exposure and the first epoch for the F555W filter and WF2 chip, which for both galaxies shows the largest background excursions. The total counts (DN) collected for the sky are given, with the number of counts for the single exposure scaled to match the exposure time of the combined frame.

Two conclusions can be drawn. First, the mean sky difference at low background levels is not zero. Inspection of the frames shows that this corresponds to a difference in the level of scattered light between the two consecutive frames due to the change in orbital position of the spacecraft. More importantly, there is a non-linear effect. A

least-squares fit to all available data points gives $\Delta s/s = (0.0094 \pm 0.0004)$ for NGC 2541, and $\Delta s/s = (0.0093 \pm 0.0002)$ for NGC 1365, where Δs is the difference in sky values between the first exposure and the first epoch of the CR-split pair (scaled to the same exposure time), and s is the sky value for the first epoch. The sense of the difference is that the sky is measured brighter in a single, CR-affected exposure, the more so the higher the background level. Notice that the agreement in the slopes measured for the NGC 2541 and NGC 1365 frames (which have exposure times differing by over a factor two) implies that the effect depends on total number of counts in the sky rather than on sky surface brightness. Responsible for this scale error is the presence, in the single exposures, of CR hits which are not flagged and therefore are folded in when calculating the background. Because hits are more easily missed on brighter backgrounds, this produces a scale error in the sky measurements. In the epoch frame, the CR hits are correctly identified and removed, and the sky is measured accurately. We therefore recommend that CR-cleaned frames be used for DoPHOT reductions whenever possible, as was done for the photometric reduction of the galaxies observed as part of the KP and the Type Ia Supernovae Calibration Project.

How does this affect the stellar magnitudes? Figure 8 shows the magnitude difference Δm between the first exposure and first epoch of the WF2 CR-split pair: these are the stars whose background is plotted in Figure 7. Given the slope of the scale error measured in the sky, and assuming that the stellar magnitudes are not affected by the presence of CRs, two stars of 25th and 27th magnitude projecting onto a sky background of 20 mag arcsec^{-2} (corresponding to 200 and 480 DN in the bottom and top panel of Figure 7 respectively) would be measured too faint by 0.01 and 0.1 mag respectively. This would produce a scale error when comparing magnitudes recovered from frames with and without CRs. No obvious scale error is however observed in Figure 8: a least square fit to the data points produces slopes $\gamma = [\Delta m/\text{input mag}]$ smaller than 0.01 mag/mag. Several causes contribute to this result. First of all, faint stars are more easily lost on brighter backgrounds. Figure 9 shows the recovery rate for stars of given magnitude as a function of backgrounds brightness. Therefore, most of the stars that would show the largest deviations, and contribute more to produce a scale error (i.e. faint stars on bright backgrounds) are not even detected. Second, just as the presence of CRs leads DoPHOT to overestimate the background brightness, it is reasonable to expect that the stars magnitudes will be somewhat overestimated as well, with the consequence that the two effects cancel, at least partially. Support to this point comes from the fact that when the difference Δm is plotted as a function of sky brightness, no obvious correlation is observed.

Figure 8 shows an increased scatter in the sense that stars are measured preferentially brighter in the single exposure than in the CR-free epoch frame. Visual inspection of the images confirms that these (the red crosses in Figure 8) are unfortunate stellar images that

happen to be hit head on by a CR. The CR is not identified in the single exposure, and the star is measured too bright. Unfortunately, these stars cannot be discriminated based on their reported error σ: for all of them $\Delta m > 4\sigma$ and their reported photometric errors are perfectly normal for their measured magnitude. Therefore, the bias would be undetected if no combined, CR-free images were available.

Is the problem solved in the case of the Key Project galaxies, for which DoPHOT is run on CR-cleaned images? Not entirely. Figure 10 shows the same red stars as in Figure 8 but this time the values plotted are the magnitude difference between the first exposure and the first epoch (in red as in Figure 8), between the second exposure and the first epoch (in black), and between the second exposure and the deep frame created by combining all available exposures (in blue). It can be readily seen that the blue points have a mean positive Δm, while the black points are well distributed around a zero Δm. We remind the reader that the stars plotted here were selected by the circumstance of having been affected by a CR in the first exposure; in very few cases will the star also have been affected by a CR in the second exposure. The fact that the black points show systematically positive magnitude residuals (by 0.10 ± 0.16 mag) argues that the procedure used in combining the first and second exposures to produce the epoch frame must leave some of the CR hit behind, so that the star is still measured brighter in the combined frame than in the second exposure. However, when all eight available frames are combined to create the deep image, the process of eliminating cosmic rays is much more effective, and the bias disappears (blue points; the weighted mean in this case is 0.01 ± 0.17). In conclusion, the simulations show that when DoPHOT is applied following the KP prescriptions, about 3% of the stars at any given epoch are measured too bright by an average of 0.1 mag. For the KP galaxies, which are observed for a total of 12 epochs, this means that about 1/3 of the Cepheids will have one out of twelve measurements biased high by 0.1 mag, which has no impact on the period-luminosity (PL) relation.

6. EFFECTS OF CONFUSION: TESTS ON THE REAL+ARTIFICIAL FRAMES

We now turn our attention to the NGC 1365 and NGC 2541 frames to which the artificial stars have been added. From now on, DoPHOT is always applied to frames which are CR-cleaned (§3), while ALLFRAME uses the original, CR-split exposures. The luminosity function of the recovered artificial stars is shown in Figures 3 and 4 by the thin yellow and blue lines for the PC and WF2 chips and the ALLFRAME and DoPHOT reductions. Figures 11 and 12 show the comparison between input and recovered

magnitudes for both ALLFRAME and DoPHOT. The results do not vary significantly from chip to chip for the same filter, and we only plot them for the WF2 chip of both NGC 1365 and NGC 2541. The same parameters listed in Table 5 for the artificial frames, i.e., the weighted mean difference between input and recovered magnitudes, and the slope of a least-squares fit line through the data, can be found in Table 6 for the real+artificial frames. Again, no significant scale errors are found, and the agreement in the zero points is within the uncertainties in the DoPHOT and ALLFRAME aperture corrections (see §3). Figures 11 and 12, however, deserve some closer inspection. The distributions show larger scatter for NGC 1365 than for NGC 2541, as expected due to the more crowded nature of the former. Unlike the control case described in §4, however, the number of points which deviate by more than three times the reported error does not follow a Gaussian distribution. In NGC 1365, 16% and 24% of the F555W and F814W DoPHOT stars brighter than 28 mag deviate by more than 3σ, in NGC 2541 the percentages are 14% and 21%. The same result, but not quite as extreme has been discussed by Saha et al. (2000), who further point out that this translates into a bias of up to 0.1 mag in the Cepheid distance moduli derived using DoPHOT in crowded fields. The plots based on ALLFRAME photometry have larger scatter, however, the photometric errors reported by ALLFRAME are larger than measured by DoPHOT, with the consequence that a smaller fraction of the ALLFRAME stars, 8% and 5% in NGC 1365 and NGC 2541 respectively, deviate by more than 3σ.

For all stars deviating by more than 3σ (the circles in Figures 11 and 12) we plot in Figure 13 the difference between the DoPHOT magnitudes measured in the first epoch and in all subsequent epochs. Because the main features of this plot repeat for all chips and both filters, we only show the case of the WF2 F814W reduction in NGC 1365. Some of the points (shown by the circles) are highly correlated. The magnitudes for these stars are mis-measured in the first epoch because of some transient event, such as the presence of a nearby hot pixel, or an undetected CR, but are measured correctly in all other epochs. While there is really no way to identify these stars in single epoch programs, in multi-epoch observations (such as Cepheid finding programs) the corrupted epoch would easily be flagged. The points shown by the crosses, however, show no obvious correlation: they scatter around a zero mean (within the uncertainties in the aperture corrections) and show no scale errors. These stars are measured systematically too bright in all of the epochs. The reason is confusion due to unresolved stellar blends or rapidly changing background level with position on the chip. Because these patterns repeat identically from epoch to epoch, they produce a bias which is impossible to detect unless artificial star experiments, of the type described in this paper, are performed in each individual case. Following Saha et al. (2000) we plot in Figures 14 to 15 the correlations between the F555W and F814W residuals for the first epoch of both galaxies, and for both ALLFRAME and DoPHOT. The results

shown for the PC and WF2 are representative of the other chips. In each figure crosses are for stars that deviate by more than 3σ in both passbands, filled and open circles for stars that deviate by more than 3σ in either F555W or F814W, and dots for well behaved stars in both bands. In all cases, we notice that there is no correlation for stars which are not affected by confusion noise (dots and circles). In Figure 13, these stars would be plotted as circles, i.e., they happen to be measured incorrectly in one particular epoch and one particular filter due to some reason that does not repeat for all other epochs (for example the vicinity of a CRs hit, or defecting pixels), and would therefore not produce a bias in the derivation of Cepheid distance moduli. However, there is a strong correlation for stars for which the difference between measured and expected magnitude is statistically larger *in both passbands* than expected given their reported photometric errors (crosses). As pointed out above, the magnitude of these stars is overestimated in each epoch and both filters, and will introduce a bias in the derived Cepheid PL relations. A quantitative discussion of the photometric biases arising from the effects described above when the photometry is performed on single frames is discussed in §6.1. Section 6.2 applies to the specific case of the Cepheid observations carried out by the KP.

6.1. Photometric Bias in Single Images

The amount of bias from confusion noise in single-epoch observations can be quantified from plots such as the ones shown in Figure 11 and 12: the bias is simply represented by how much, in the mean, the recovered magnitudes differ from the input magnitudes. This is estimated by:

• defining a robust weighted mean $\overline{\Delta m}_{true}$ of the difference between input and recovered magnitudes in the real+artificial frames as described in §4. Only bright, isolated, and therefore well measured stars contribute to $\overline{\Delta m}_{true}$, which therefore represents the 'true' value of the mean for any sample of stars in the absence of biases;

• computing a straight mean $\overline{\Delta m}_{bias}$ of all available data points recovered in the real+artificial frames;

• calculating the difference $\epsilon = \overline{\Delta m}_{true} - \overline{\Delta m}_{bias}$. This represents the amount of bias for single epoch observations, and is listed in Table 7.

We note that while for single epoch one band photometry of crowded fields ALLFRAME is more affected by confusion noise than DoPHOT (Table 7), ALLFRAME was specifically designed to take optimum advantage of the information content of multi-filter, multi-epoch observations, such as searches for variable stars. While ALLFRAME shows larger scatter

than DoPHOT in Figures 11 and 12, the deviant points have large photometric errors in ALLFRAME, which is not the case for DoPHOT. While it would be difficult to discriminate against these stars in individual exposures (apart from rejecting them on the basis of their large errorbars), the problem is lessened in most practical cases: photometric observations often involve multiple filters, for example, and for Cepheids observations carried out using the KP procedure, the large photometric errors attached to the ALLFRAME magnitudes would prevent one from selecting most of the deviant stars as Cepheid variables.

6.2. Photometric Bias in the Extragalactic Distance Scale

For multi-epoch programs such as observations of Cepheid variables, the bias discussed in §6.1 is somewhat lessened. This is because some of the deviant stars will be flagged once the photometry obtained for consecutive exposure or in different filters is compared. Let us consider the case of the galaxies observed by the KP, whose goal is to discover Cepheids and measure their period and mean magnitudes. Observation in two filters and multiple epochs are available. First of all, we pointed out already that stars which deviate in *only one* of the filters by more than three times their reported error (Figures 14 and 15) are corrupted by a transient phenomenon (for example a cosmic ray) affecting that particular epoch, but none of the others. When comparing photometry from different epochs, the corrupted measurement would easily be flagged (this would correspond, for example, to an obviously deviant point in an otherwise well phased light curve). We can therefore remove the corrupted measurements from our sample. Second, fits to the Cepheid PL relation are not weighted, however Cepheids which deviate from the ridge-line of the PL relation by a significant amount (generally three times the intrinsic 1σ width of the relation) are rejected. The KP adopted $1\sigma = 0.27$ mag in V and $1\sigma = 0.18$ mag in I for the PL relation. When calculating the bias introduced by confusion noise in the Cepheid sample we do the following (the artificial star magnitudes in this case can be related to the Cepheids mean magnitudes):

• include in the sample only measurements that deviate from the straight mean of all data points by more *or* less than three times their reported error in *both* F555W or F814W. This addresses the first point mentioned above. Farther reduce the sample by excluding all stars which deviate from the mean by more than 0.81 mag in F555W and more than 0.54 mag in F814W. This addresses the second point above and flags only a few of the most extreme points.

• For this sample, calculate $\overline{\Delta m}_{true}$ as done in the case of single-epoch observations. Effectively, because $\overline{\Delta m}_{true}$ is a robust weighted mean, the prior exclusion of the data

satisfying the conditions above has no effects.

• For the same sample, calculate the mean difference $\overline{\Delta m}_{bias}$ between input and recovered magnitudes. Given the distances to NGC 2541 and NGC 1365, and the fact that the maximum period (and therefore maximum mean magnitude) of the Cepheids is constrained by the length of the observing window (60 days), the range in V magnitudes spanned by the Cepheids is $24.3 < m_V << 28$ mag and $25.1 < m_V << 28$ mag in NGC 2541 and NGC 1365 respectively (Ferrarese et al. 1998, Silbermann et al. 1999). Only these magnitude ranges are therefore considered in calculating $\overline{\Delta m}_{bias}$. Notice that the exclusion of the brighter, least biased, part of the distribution in Figures 11 and 12, and the inclusion of the faint tail up to $m_V = 28$ mag (when in fact few Cepheids ever get fainter than 27.5 mag) leads to an increase in $\overline{\Delta m}_{bias}$, compared to the case in which the entire wavelength range were to be used.

• Finally, calculate the difference $\epsilon = \overline{\Delta m}_{true} - \overline{\Delta m}_{bias}$. This is the bias due to confusion noise expected in the *apparent* Cepheid distance moduli, and is listed in Table 8.

The bias in the *final*, dereddened distance modulus is given by $\delta\mu_0 \sim \epsilon_V$ when the magnitudes in both V and I passbands are mis-measured by approximately the same amount (i.e. the correlations of residuals in Figures 14 and 15 has a unit slope) (Saha et al. 2000). From Table 8, the first conclusion is that even for the most crowded fields, i.e. WF2 of NGC 1365, the bias is not larger than 0.07-0.08 mag, in agreement with the findings by Saha et al. (2000) in the very crowded field of NGC 4639 (the authors estimate the bias to be less than 0.08 mag). In the specific example of NGC 1365, for which Silbermann et al. (1999) derived a distance modulus of 31.31± 0.20 (random) ± 0.18 (systematic) based on ALLFRAME photometry, the bias estimated from a mean of all four chips in Table 8 would be ~ 0.025 mag, and can be easily neglected. In the less crowded fields of more nearby galaxies, such as NGC 2541, the bias is further reduced.

There is an additional factor which, while not easily quantifiable, will farther decrease the already insignificant amount of bias in the Cepheid distance modulus. Contamination by an underlying companion would artificially decrease the amplitude of the Cepheid light curve, and either lead to a reduction of confidence in the light curve, or preclude detection as a variable star altogether. We have conducted experiments by adding increasing amount of contamination to real Cepheid light curves observed by the Key Project Team. While we could not discriminate against Cepheids for which the contamination amounts to 30% or less of the Cepheid mean flux, in most cases the Cepheids were recognized as affected when the contamination level was increased beyond 60%.

One last points needs to be discussed. The bias calculated above can be considered

representative of the bias affecting the Cepheid sample, and therefore the Cepheid distance modulus, only if the artificial stars and the Cepheids are affected by the same level of crowding. Figure 16 shows the mean and rms contamination affecting the sample of Cepheids (solid circles and smaller errorbars) and artificial stars (open circles and larger errorbars) as a function of F555W magnitudes. To calculate the quantity on the y-axis, we counted the number of real stars detected within a 5 pixel radius of each Cepheid and artificial star. We then calculated the ratio between the total flux contributed by these nearby companions to the flux of the central star. We refer to this quantity, multiplied by 100, as the 'percent contamination': its mean and standard deviation, binned in 0.5 magnitude intervals, are plotted as a function of the F555W magnitude of the central star in Figure 16, for both NGC 2541 and NGC 1365. In making the plot, we used the real sample of Cepheids from which a distance was derived (from Ferrarese et al. 1998 and Silbermann et al. 1999). So, for example, the total flux of the stars within a 5 pixel radius of the NGC 2541 Cepheids with F555W magnitudes between 24.5 and 25.0 is equal, in the mean, to $f_c/f = (4 \pm 5)\%$ the flux of the Cepheid. In the same magnitude range, $f_c/f = (5 \pm 12)\%$ for the artificial stars. It is easy to see from the figure that, if anything, the artificial stars are *more* contaminated than the Cepheids. Therefore the bias listed in table 8 can be considered as a hard upper limit to the amount of bias affecting the Cepheid sample, and the derived Cepheid distances.

The results of the tests presented in this work are at odds with the finding of Mochejska et al. (1999) and Stanek & Udalski (1999), who speculate from the analysis of Cepheids in LMC and M31 fields that the Cepheid distances published by the KP and the Type Ia Supernovae Calibration Team are underestimated by up to 15% (0.3 mag) due to neglecting the effects of blending. The Mochejska et al. and Stanek & Udalski analysis, while correctly assuming that unresolved blending will artificially increase a star's magnitude, do not consider that for the same reason the underlying sky will be brightened. The interplay of the two effects cannot be estimated unless the photometry is actually *performed on* (as opposed to extrapolated to) the distant galaxy fields, using some kind of control test which in our case is provided by the artificial stars. In addition, Mochejska et al. and Stanek & Udalski assume that the stellar background in the LMC and M31 fields is representative of the more distant fields observed with HST, when in fact it is significantly brighter.

7. PHOTOMETRIC ZERO POINT TEST: DoPHOT

The tests discussed so far say very little about the accuracy of the DoPHOT or ALLFRAME zero points, since the artificial star magnitudes are based on the ALLFRAME

photometric calibration. The DoPHOT zero point was tested for the most crowded of the fields considered, the WF2 chip of NGC 1365, using as 'artificial stars' a real field observed in the dwarf local group galaxy Sextans A. The Sextans A images used were obtained as part of program GO-5915 on December 1, 1995, for a total of 1800 seconds of integration in both F555W and F814W filters. Based on §4, we expect the magnitudes reported by DoPHOT when run on this uncrowded field to be very accurate. A comparison between these magnitudes, and the magnitudes recovered when the Sextans A field is added to the F555W WF2 NGC 1365 frame is shown in Figure 17. A weighted fit to all stars gives perfect agreement in the absolute zero points, $\Delta(m) = 0.000 \pm 0.065$, and no scale error.

8. SUMMARY OF CONCLUSIONS

We have discussed the performance of the DoPHOT and ALLFRAME photometric procedures when applied to crowded fields observed with the WFPC2 on board *HST*. We have focused on searching for biases that can affect the determination of the Cepheid distance moduli derived by the *HST* Key Project on the Extragalactic Distance Scale and the Type Ia Supernovae Calibration Project, but our results are relevant for any photometric study requiring high precision measurements. The following conclusions and guidelines are the results of this paper.

• When doing any photometric analysis, tests should be performed to asses the impact of CR events on the photometry. In the case of DoPHOT, it is highly recommended to use frames from which CRs have been removed. When CRs are present, DoPHOT has a tendency to overestimate the sky brightness by amounts that can be significant when total counts per pixel in the sky exceed a few hundred DN. The problem is completely solved only when several exposures are available and the photometry is obtained from an image created by combining all exposures. In the specific case of most of the galaxies observed as part of the *HST* Key Project, where only two exposures are available for each epoch of observation, the stars affected are different in each epoch and are not present in a large enough number to introduce a bias in the derived Cepheid distance modulus. The effects of CRs on the ALLFRAME photometry remain to be tested, however given the good agreement between the ALLFRAME and DoPHOT photometry obtained for all KP galaxies (better than 0.05 mag, or well within the uncertainties in the aperture corrections), it is unlikely that CRs introduce a significant bias, if any.

• Both DoPHOT and ALLFRAME perform extremely well, both in recovering magnitudes and in estimating their errors, in uncrowded fields with limited variation in the background brightness across the chip.

• In crowded fields, such as the ones observed by the *HST* Key Project team, a bias is introduced by the presence of confusion noise due to crowding and rapidly varying background levels across the chip. This is in the sense that a fraction ($\sim$ 5-10% for ALLFRAME and up to 25% for DoPHOT) of the stars are measured consistently too bright. The effect on the photometry of single epoch observations can be significant, 0.05 mag even for not too crowded fields, such as the WF4 chip of NGC 2541, and up to 0.2 mag for the most crowded and distant fields observed by the KP, such as NGC 1365. The bias is somewhat worse when ALLFRAME, rather than DoPHOT photometry is used. When the photometry is applied to derive Cepheid distance moduli from multi-epoch observations, however, the bias is significantly reduced because strict criteria are imposed in selecting the variable stars. In the case of ALLFRAME, the bias in the final distance modulus is negligible, leading to underestimate the distance by 1% (0.02 mag) at most for the most crowded and distant fields observed by the *HST* Key Project. The effects is slightly larger, $\sim$ 2% mag, when DoPHOT photometry is used, but is in no case as large as extrapolated by Mochejska et al. (1999) and Stanek & Udalski (1999) from ground based studies of M31 and LMC fields.

We wish to thank the anonymous referee for the useful suggestions that helped improve the quality of this manuscript. LF acknowledges support by NASA through Hubble Fellowship grant HF-01081.01-96A and through Long Term Space Astrophysics program NRA-98-03-LTSA-03.

A. An Empirical Test of the Effects of Crowding on the Distance Scale

We have concluded that the Key Project distance scale is compressed by photometric confusion problems by no more than 0.025 mag. It is interesting to consider whether there is any way of checking that *a posteriori*.

One possibility is to examine residuals from the Tully Fisher relation and to seek correlations with distance. If distances for remote galaxies are underestimated due to their higher probability of image blending (Stanek & Udalski 1999), those galaxies would lie low in the Tully Fisher diagram of Sakai et al. (2000), as also pointed out by Gibson et al. (2000).

Figure 18 shows H-band residuals from Sakai's equation (10) plotted against distance. Such correlation as there is is in the opposite sense. In fact, calculating the slope in Figure 18 and its uncertainty, we can rule out the *positive* correlation one might expect due to blending at the 1.85σ level. This supports our conclusion that the Key Project distance

scale is not compressed by photometric confusion problems by more than 0.025 mag, a conclusion also reached by Gibson et al.

REFERENCES

Ferrarese, L., et al. 1996, ApJ, 464, 568

Ferrarese, L., et al. 1998, ApJ, 507, 655

Gibson, B. K., Maloney, P. R., & Sakai, S. 2000, ApJL, submitted

Hill, R., et al. 1998, ApJ, 496, 648

Holtzmann, J. A. et al. 1995, PASP, 107, 1065

Kennicutt, R. C., Freedman, W. L., & Mould, J. R. 1995, AJ, 110, 1476

Mochejska, B. J., Macri, L. M., Sasselov, D. D., & Stanek, K. Z. 1999, astro-ph/9908293

Saha, A., Labhardt, L., Schwengeler, H., Macchetto, F. D., Panagia, N., Sandage, A. & Tammann, G. A. 1994, ApJ, 425, 14

Saha, A., Sandage, A. & Tammann, G. A., Labhardt, L., Macchetto, F. D., Panagia, N. 1997, ApJ, 486, 1

Saha, A., Labhardt, L., & Prosser, C. 2000, PASP, in press

Sakai, S., et al. 2000, ApJ, in press (astro-ph/9909269)

Sandage, A., et al. 1992, ApJL, 401, 7

Schechter, P. L., Mateo, M., & Saha, A. 1993, PASP, 105, 1342

Silbermann, N. A. et al. 1999, ApJ, 515, 1

Stanek, K. Z., & Udalski, A. 1999, astro-ph/9909346

Stetson, P. B. 1990, PASP, 102, 932

Stetson, P. B. 1994, PASP, 106, 250

Stetson, P. B. 1998, PASP, 110, 1448

Whitmore, B., & Heyer, I. 1997, Instrument Science Report WFPC2 97-08 (Baltimore: STScI)

Table 1. Data Files

Description[1]	Rootname	t_{exp}(s)	Filter	Date Obs.
–NGC 2541–				
1st V epoch, 1st exposure	U2S72901T	1100	F555W	30/10/95
1st V epoch, 2nd exposure	U2S72902T	1100	F555W	30/10/95
1st I epoch, 1st exposure	U2S72903T	1300	F814W	30/10/95
1st I epoch, 2nd exposure	U2S72904T	1300	F814W	30/10/95
2nd V epoch, 1st exposure	U2S73001T	1100	F555W	5/11/95
2nd V epoch, 2nd exposure	U2S73002T	1100	F555W	5/11/95
2nd I epoch, 1st exposure	U2S73003T	1300	F814W	5/11/95
2nd I epoch, 2nd exposure	U2S73004T	1300	F814W	5/11/95
3rd V epoch, 1st exposure	U2S73402T	900	F555W	20/11/95
3rd V epoch, 2nd exposure	U2S73403T	900	F555W	20/11/95
3rd I epoch, 1st exposure	U2S73405T	1100	F814W	20/11/95
3rd I epoch, 2nd exposure	U2S73406T	1100	F814W	20/11/95
4th V epoch, 1st exposure	U2S73901T	1100	F555W	8/12/95
4th V epoch, 2nd exposure	U2S73902T	1100	F555W	8/12/95
4th I epoch, 1st exposure	U2S73903T	1300	F814W	8/12/95
4th I epoch, 2nd exposure	U2S73904T	1300	F814W	8/12/95
–NGC 1365–				
1st V epoch, 1st exposure	U2S71201T	2400	F555W	19/09/95
1st V epoch, 2nd exposure	U2S71202T	2700	F555W	19/09/95
1st I epoch, 1st exposure	U2S71203T	2700	F814W	19/09/95
1st I epoch, 2nd exposure	U2S71204T	2700	F814W	19/09/95
2nd V epoch, 1st exposure	U2S70201T	2400	F555W	6/08/95
2nd V epoch, 2nd exposure	U2S70202T	2700	F555W	6/08/95
2nd I epoch, 1st exposure	U2S70203T	2700	F814W	6/08/95
2nd I epoch, 2nd exposure	U2S70204T	2700	F814W	6/08/95
3rd V epoch, 1st exposure	U2S70301T	2400	F555W	14/08/95
3rd V epoch, 2nd exposure	U2S70302T	2700	F555W	14/08/95
3rd I epoch, 1st exposure	U2S70303T	2700	F814W	14/08/95
3rd I epoch, 2nd exposure	U2S70304T	2700	F814W	14/08/95
4th V epoch, 1st exposure	U2S70701T	2400	F555W	29/08/95
4th V epoch, 2nd exposure	U2S70703T	2300	F555W	29/08/95
4th I epoch, 1st exposure	U2S70705T	2300	F814W	29/08/95
4th I epoch, 2nd exposure	U2S70706T	2700	F814W	29/08/95

[1]The complete time sequence observed by the KP for NGC 2541 and NGC 1365 comprises a total of 12 epochs. The ones considered here have been labeled first to fourth for convenience.

Table 2. DoPHOT PSF Parameters

	PC			WF2			WF3			WF4		
	Δ_{maj} (pix)	Δ_{min} (pix)	Tilt	Δ_{maj} (pix)	Δ_{min} (pix)	Tilt	Δ_{maj} (pix)	Δ_{min} (pix)	Tilt	Δ_{maj} (pix)	Δ_{min} (pix)	Tilt
–NGC1365, F555W–												
Real frame	1.382	1.318	30°.62	1.275	1.262	−22°.80	1.272	1.226	21°.16	1.260	1.140	−68°.44
Artificial frame	1.271	1.109	37°.71	1.174	1.130	−20°.81	1.328	1.224	37°.23	1.299	1.159	−67°.72
Real+art., 1st exp.	1.257	1.138	32°.97	1.168	1.133	−42°.76	...	...	...	...	...	...
Real+art., 1st epoch	1.274	1.163	33°.65	1.159	1.114	−39°.15	1.263	1.165	31°.70	1.251	1.120	−68°.35
–NGC1365, F814W–												
Real frame	3.924	3.819	39°.14	1.291	1.226	80°.99	1.299	1.223	1°.96	1.313	1.213	−80°.03
Artificial frame	3.987	3.837	43°.42	1.160	1.143	75°.78	1.246	1.161	32°.03	1.240	1.153	−72°.04
Real+art., 1st exp.	3.810	3.734	42°.62	1.206	1.175	−74°.43	...	...	...	...	...	...
Real+art., 1st epoch	3.856	3.761	48°.32	1.196	1.166	88°.76	1.217	1.154	34°.38	1.223	1.144	−76°.32
–NGC2541, F555W–												
Real frame	1.198	1.118	37°.35	1.195	1.112	−36°.04	1.199	1.122	17°.37	1.226	1.074	−70°.42
Artificial frame	1.247	1.111	39°.05	1.171	1.123	−30°.70	1.329	1.221	31°.99	1.285	1.151	−64°.45
Real+art., 1st exp.	1.268	1.127	34°.42	1.149	1.113	−20°.23	...	...	...	...	...	...
Real+art., 1st epoch	1.273	1.144	35°.21	1.145	1.113	−26°.46	1.255	1.164	30°.92	1.201	1.092	−63°.09
–NGC2541, F814W–												
Real frame	3.764	3.651	42°.69	1.189	1.151	−47°.64	1.185	1.148	13°.28	1.206	1.107	−72°.35
Artificial frame	4.010	3.848	44°.99	1.158	1.148	−49°.09	1.227	1.169	27°.21	1.225	1.156	−67°.85
Real+art., 1st exp.	3.870	3.733	41°.85	1.152	1.131	6°.67	...	...	...	...	...	...
Real+art., 1st epoch	3.898	3.753	41°.58	1.163	1.156	−85°.61	1.191	1.154	36°.68	1.218	1.135	−76°.48

Table 3. DoPHOT Aperture Corrections

	PC (mag)[1]	WF2 (mag)[1]	WF3 (mag)[1]	WF4 (mag)[1]
–F555W–				
LeoI values	−0.880	−0.703	−0.614	−0.6821
N2541, real+art. 1st epoch	−0.869±0.003 (262)	−0.714±0.005 (175)	−0.618±0.004 (220)	−0.712±0.004 (210)
N2541, real+art. 1st exposure	−0.880±0.005 (151)	−0.713±0.007 (111)	... [2]	... [2]
N2541, artificial frame	−0.872±0.002 (524)	−0.683±0.001 (737)	−0.581±0.001 (558)	−0.682±0.002 (535)
N1365, real+art. 1st epoch	−0.891±0.005 (138)	−0.693±0.008 (80)	−0.617±0.006 (156)	−0.708±0.006 (97)
N1365, real+art. 1st exposure	−0.892±0.011 (34)	−0.730±0.02 (27)	... [2]	... [2]
N1365, artificial frame	−0.869±0.002 (610)	−0.677±0.001 (726)	−0.579±0.001 (730)	−0.685±0.001 (662)
–F814W–				
LeoI values	1.066	−0.740	−0.763	−0.7641
N2541, real+art. 1st epoch	1.081±0.003 (423)	−0.734±0.004 (219)	−0.755±0.003 (271)	−0.773±0.003 (263)
N2541, real+art. 1st exposure	1.079±0.005 (136)	−0.757±0.008 (64)	... [2]	... [2]
N2541, artificial frame	1.107±0.001 (558)	−0.739±0.001 (802)	−0.739±0.001 (724)	−0.763±0.001 (712)
N1365, real+art. 1st epoch	1.059±0.005 (210)	−0.766±0.008 (96)	−0.754±0.004 (219)	−0.780±0.006 (140)
N1365, real+art. 1st exposure	1.041±0.013 (30)	−0.814±0.028 (18)	... [2]	... [2]
N1365, artificial frame	1.105±0.001 (697)	−0.740±0.001 (784)	−0.735±0.001 (861)	−0.763±0.001 (763)

[1]The aperture corrections are based on the number of stars shown in parentheses.

[2]DoPHOT was run on single exposures (to test for biases introduced by CR hits) only for the PC and WF2.

Table 4. ALLFRAME Aperture Corrections

	PC (mag)[1]	WF2 (mag)[1]	WF3 (mag)[1]	WF4 (mag)[1]
–F555W–				
N2541 1st exp.	0.009±0.012 (21)	0.007±0.0085 (24)	0.040±0.011 (21)	0.023±0.020 (13)
N2541 2nd exp.	−0.023±0.011 (23)	−0.012±0.0090 (23)	0.021±0.013 (19)	−0.009±0.023 (10)
N1365 1st exp.	−0.186±0.043 (13)	−0.046±0.025 (16)	−0.011±0.035 (8)	−0.082±0.023 (18)
N1365 2nd exp.	−0.166±0.031 (10)	−0.036±0.026 (16)	−0.001±0.036 (9)	−0.082±0.022 (18)
–F814W–				
N2541 1st exp.	0.013±0.012 (18)	0.047±0.0084 (23)	0.090±0.010 (22)	0.069±0.014 (17)
N2541 2nd exp.	0.032±0.012 (16)	0.022±0.0083 (22)	0.037±0.010 (20)	0.038±0.015 (15)
N1365 1st exp.	−0.063±0.024 (9)	−0.031±0.024 (13)	0.023±0.035 (10)	0.058±0.025 (12)
N1365 2nd exp.	−0.342±0.111 (9)	−0.039±0.028 (14)	−0.008±0.031 (10)	0.047±0.021 (13)

[1]The aperture corrections are based on the number of stars shown in parentheses.

Table 5. Control Test on the NGC 1365 Artificial Frames

	DoPHOT		ALLFRAME	
	$\Delta m \pm \sigma(\Delta m)$ (mag)	$\gamma \pm \sigma(\gamma)$ (mag/mag)	$\Delta m \pm \sigma(\Delta m)$ (mag)	$\gamma \pm \sigma(\gamma)$ (mag/mag)
PC, F555W	-0.20 ± 0.04	-0.0010 ± 0.0010	0.00 ± 0.03	0.0013 ± 0.0006
WF2, F555W	-0.04 ± 0.03	-0.0020 ± 0.0008	0.01 ± 0.03	0.0006 ± 0.0006
PC, F814W	-0.08 ± 0.04	-0.0018 ± 0.0009	0.00 ± 0.03	0.0004 ± 0.0006
WF2, F814W	-0.08 ± 0.03	-0.0009 ± 0.0007	0.00 ± 0.03	0.0008 ± 0.0006

Table 6. Photometric Test on the Real+Artificial Frames

	DoPHOT		ALLFRAME	
	$\Delta m \pm \sigma(\Delta m)$ (mag)	$\gamma \pm \sigma(\gamma)$ (mag/mag)	$\Delta m \pm \sigma(\Delta m)$ (mag)	$\gamma \pm \sigma(\gamma)$ (mag/mag)
–N1365–				
PC, F555W	0.12 ± 0.05	-0.0009 ± 0.0014	0.01 ± 0.05	0.0007 ± 0.0016
WF2, F555W	0.02 ± 0.05	0.0019 ± 0.0015	0.03 ± 0.10	-0.0022 ± 0.0031
WF3, F555W	0.02 ± 0.04	0.0025 ± 0.0011	0.00 ± 0.04	0.0012 ± 0.0014
WF4, F555W	-0.05 ± 0.05	0.0014 ± 0.0013	0.01 ± 0.05	0.0026 ± 0.0018
PC, F814W	-0.02 ± 0.06	0.0013 ± 0.0018	0.01 ± 0.04	0.0023 ± 0.0016
WF2, F814W	0.07 ± 0.06	0.0015 ± 0.0019	0.03 ± 0.07	0.0009 ± 0.0025
WF3, F814W	0.09 ± 0.04	0.0006 ± 0.0011	0.00 ± 0.04	-0.0010 ± 0.0013
WF4, F814W	0.10 ± 0.04	-0.0015 ± 0.0013	0.00 ± 0.04	0.0014 ± 0.0015
–N2541–				
PC, F555W	0.02 ± 0.05	0.0005 ± 0.0013	0.09 ± 0.05	-0.0009 ± 0.0013
WF2, F555W	0.04 ± 0.04	0.0000 ± 0.0012	0.01 ± 0.07	-0.0053 ± 0.0021
WF3, F555W	0.07 ± 0.04	0.0017 ± 0.0011	0.01 ± 0.05	-0.0007 ± 0.0014
WF4, F555W	0.02 ± 0.05	-0.0004 ± 0.0012	0.00 ± 0.04	-0.0034 ± 0.0013
PC, F814W	0.00 ± 0.03	-0.0002 ± 0.0009	0.00 ± 0.03	-0.0007 ± 0.0010
WF2, F814W	0.01 ± 0.04	0.0023 ± 0.0012	0.01 ± 0.05	-0.0022 ± 0.0015
WF3, F814W	0.08 ± 0.04	0.0019 ± 0.0010	0.00 ± 0.03	-0.0011 ± 0.0011
WF4, F814W	0.02 ± 0.03	0.0009 ± 0.0009	0.00 ± 0.04	-0.0002 ± 0.0010

Table 7. Bias Affecting Stars in Single Epoch Photometry

Chip	DoPHOT		ALLFRAME	
	ϵ_V (mag)	ϵ_I (mag)	ϵ_V (mag)	ϵ_I (mag)
–N1365–				
PC	0.069	0.066	0.124	0.134
WF2	0.138	0.179	0.207	0.191
WF3	0.074	0.072	0.119	0.124
WF4	0.082	0.107	0.158	0.166
–N2541–				
PC	0.040	0.041	0.034	0.080
WF2	0.088	0.118	0.121	0.145
WF3	0.039	0.043	0.051	0.098
WF4	0.041	0.037	0.049	0.068

Table 8. Bias Affecting the Cepheid Apparent Distance Moduli

Chip	DoPHOT		ALLFRAME	
	ϵ_V (mag)	ϵ_I (mag)	ϵ_V (mag)	ϵ_I (mag)
–N1365–				
PC	0.040	0.037	0.026	0.021
WF2	0.086	0.075	0.036	0.056
WF3	0.033	0.041	0.021	0.018
WF4	0.055	0.056	0.026	0.031
–N2541–				
PC	0.027	0.027	0.000	0.017
WF2	0.063	0.067	0.037	0.028
WF3	0.023	0.011	0.009	0.021
WF4	0.031	0.018	0.022	0.013

Fig. 1.— Top: A CR-free image of the NGC 1365 field obtained by combining the eight F555W exposures in Table 1. Bottom: the artificial star frame added to the NGC 1365 field. The two images are displayed with the same grey-scale, to preserve the brightness ratio of the real and artificial stars.

Fig. 2.— As for Figure 1, but for the NGC 2541 field.

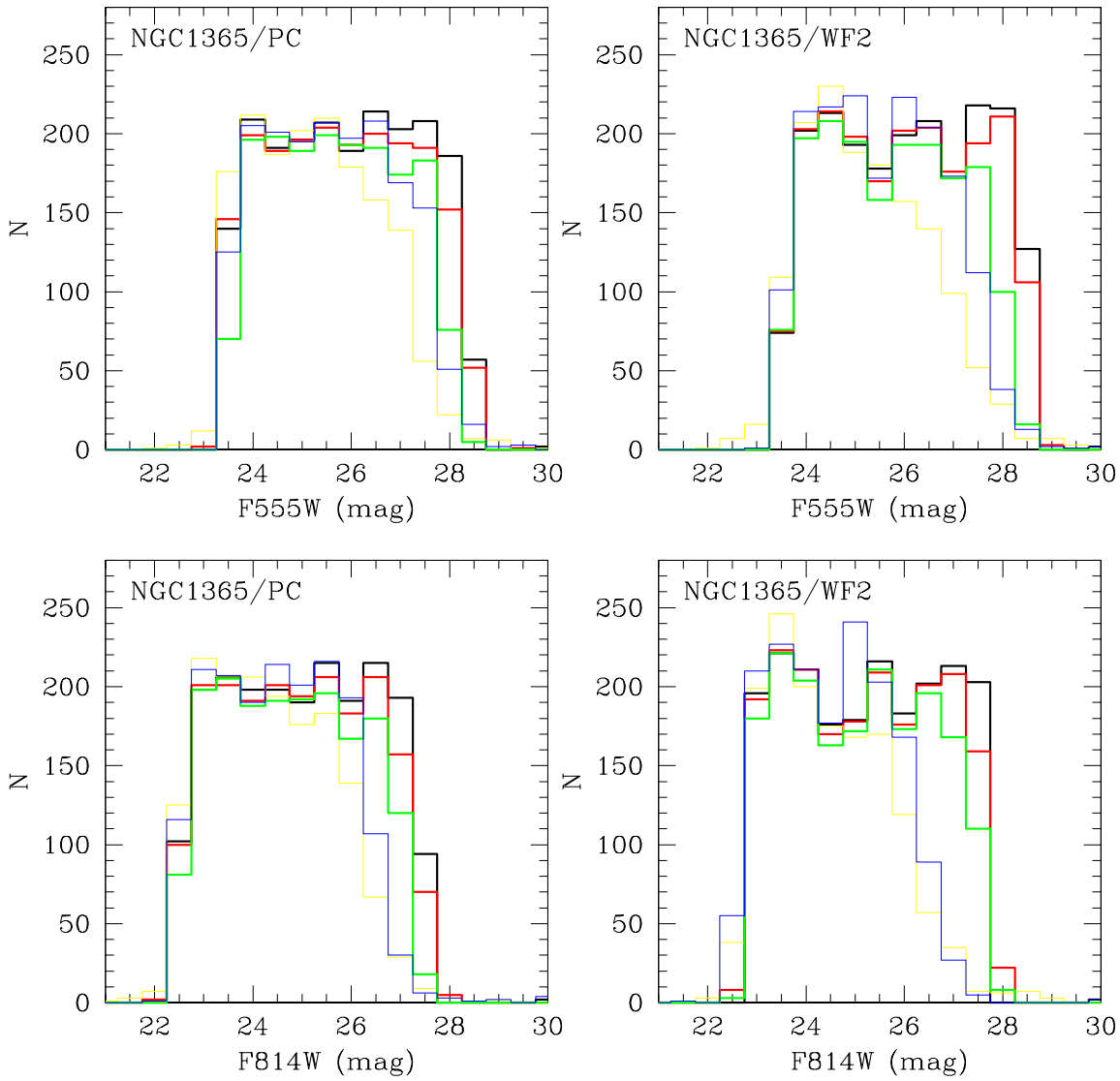

Fig. 3.— Luminosity function (LF) of the input and recovered stars in the PC and WF2 NGC 1365 fields. The input LF is in black. The LF's recovered from the frames containing only the artificial stars by ALLFRAME and DOPHOT are shown by the thick red and green lines respectively. The thin yellow and blue lines are the LF's for the artificial stars recovered by ALLFRAME and DoPHOT respectively in the artificial+real star frames. The photometry for the first exposure, U2S71201T, was used for ALLFRAME, and for the first epoch (U2S71201T and U2S71201T combined) for DoPHOT).

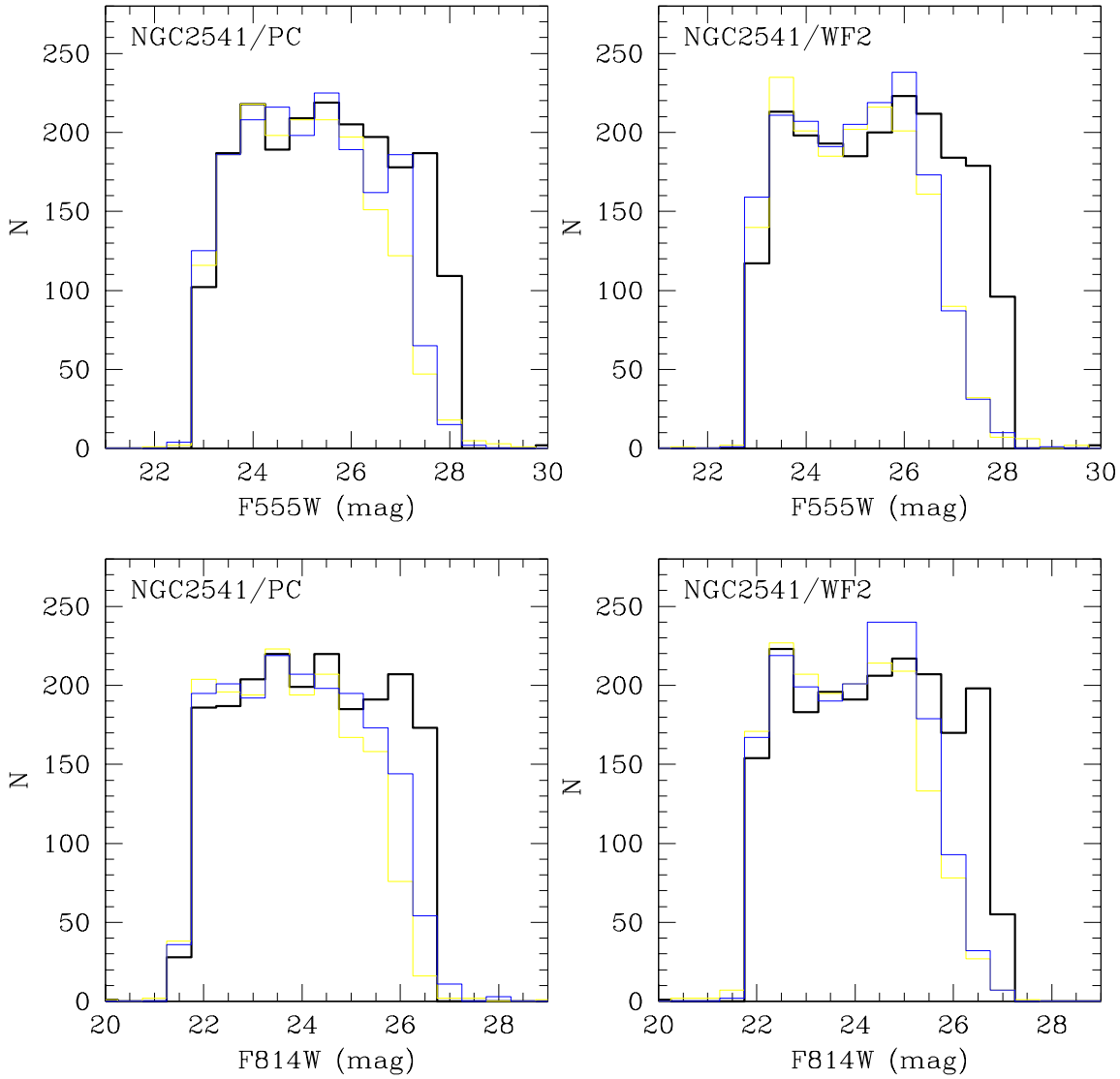

Fig. 4.— As Figure 3, but for the NGC 2541 field. The luminosity functions recovered from the artificial star frames are not shown. The photometry used for the real+artificial star frames is from US72901T for ALLFRAME, and the first epoch (US72901T and US72902T combined) for DoPHOT.

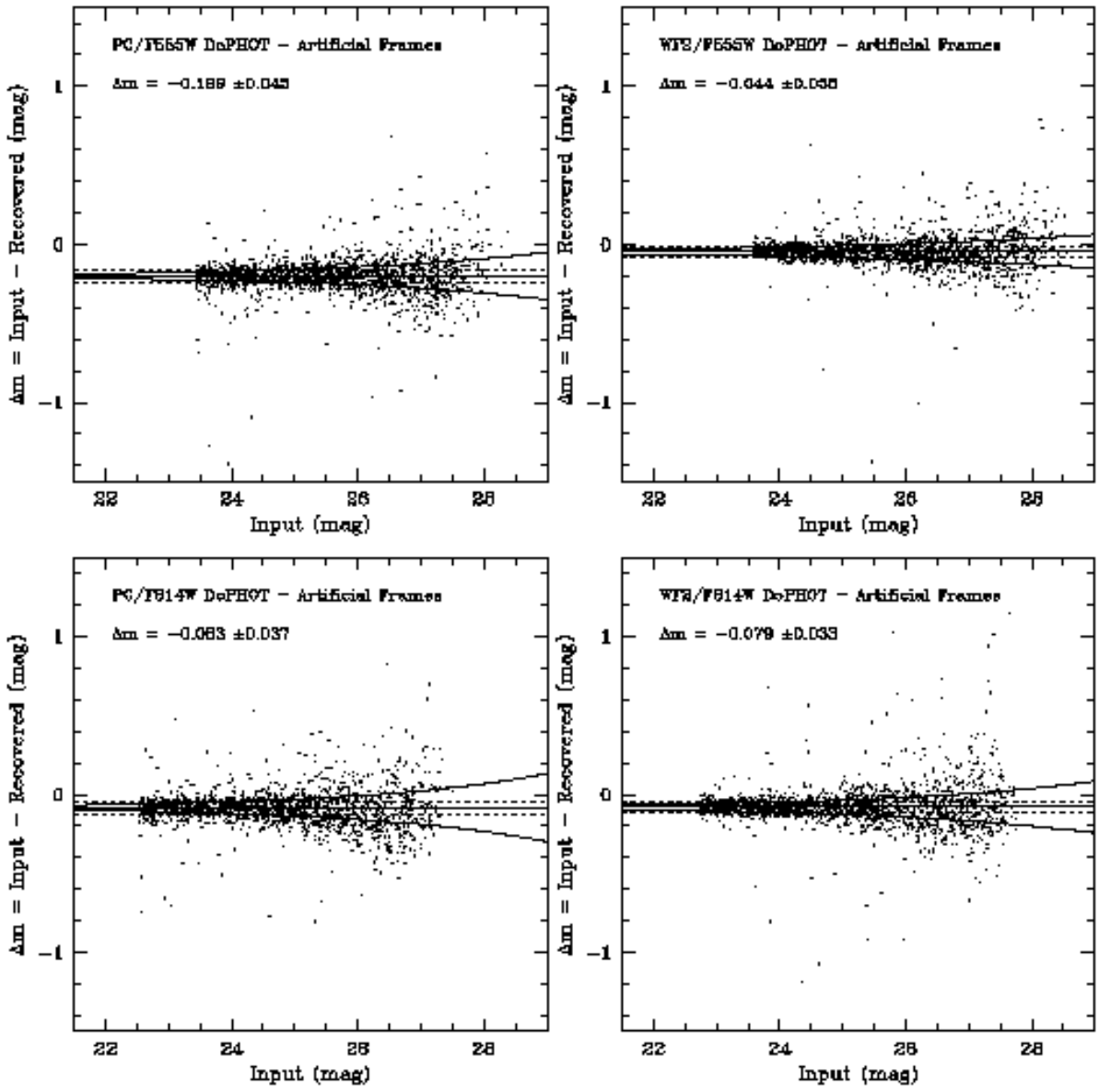

Fig. 5.— Difference between the input magnitudes and the magnitudes recovered by DoPHOT from the artificial star frames. The exponential curves represent the typical error reported by DoPHOT for a star of the magnitude shown in the abscissa. The solid and dotted straight lines are the weighted mean and 1σ deviations calculated as explained in the text.

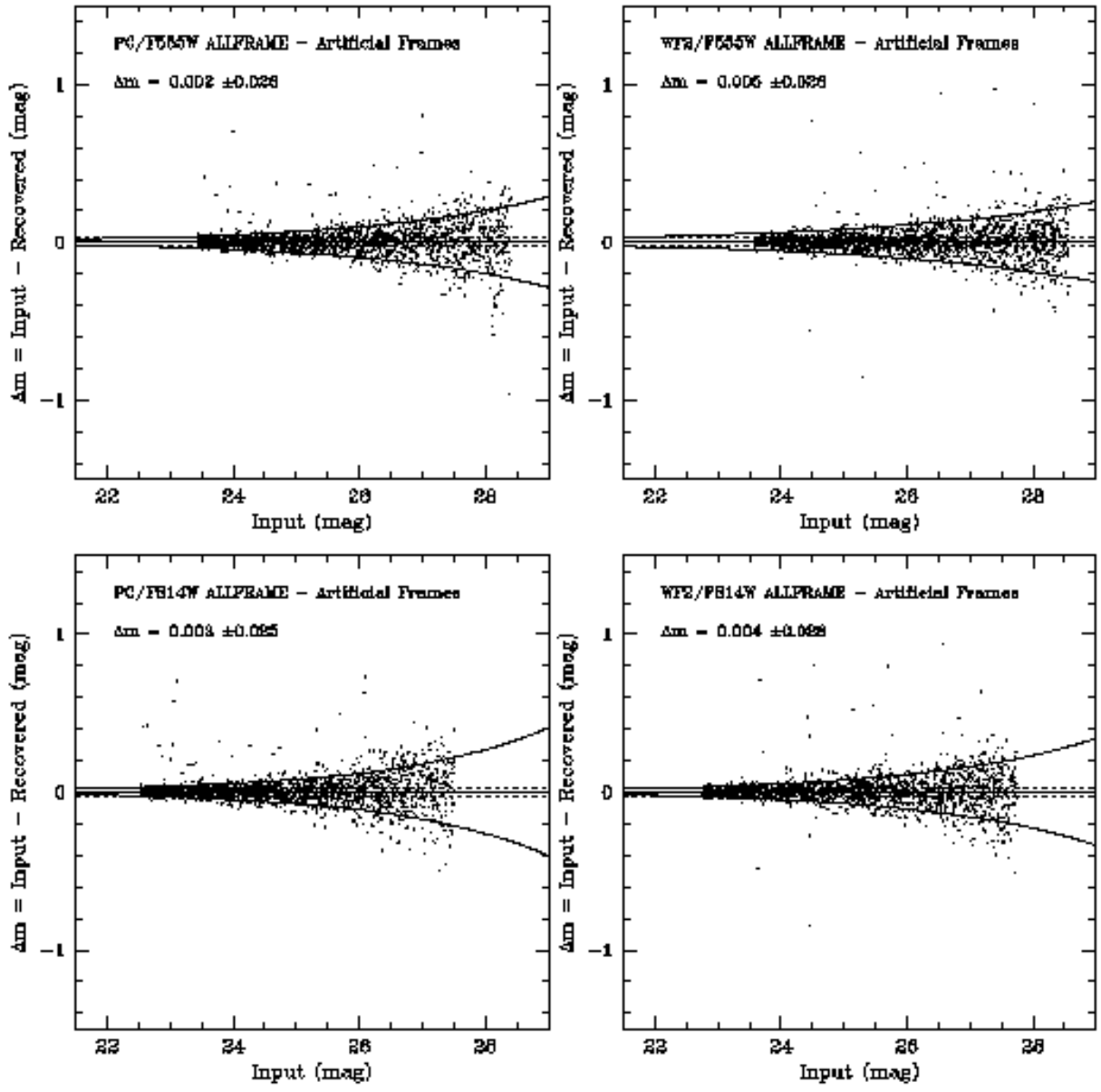

Fig. 6.— As Figure 5, but for the ALLFRAME reduction.

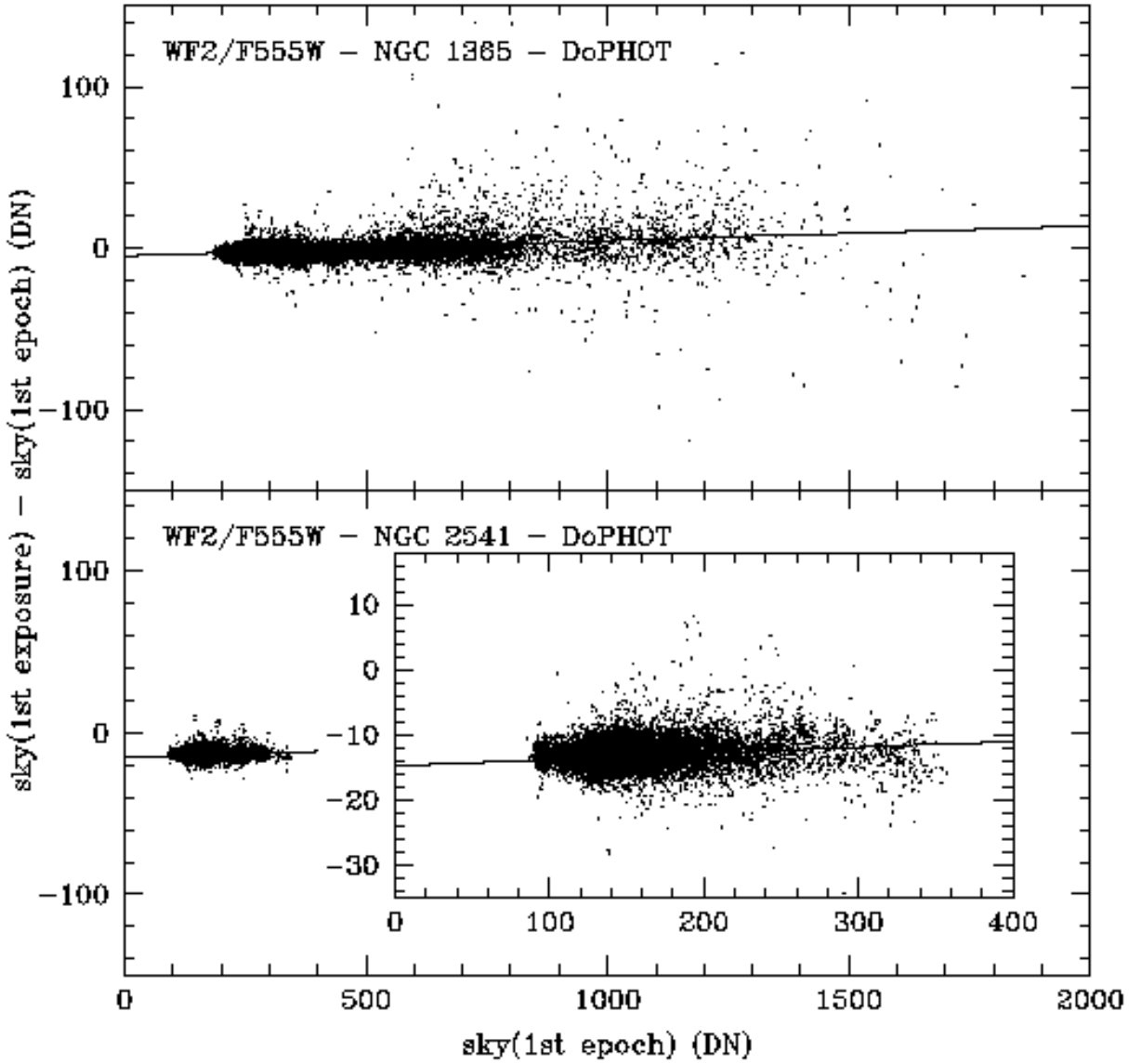

Fig. 7.— Difference in the sky values measured by DoPHOT for the stars in the first exposure and first epoch (first and second exposure combined) of NGC 1365 (top) and NGC 2541 (bottom). The solid line is a least-squares fit to the data.

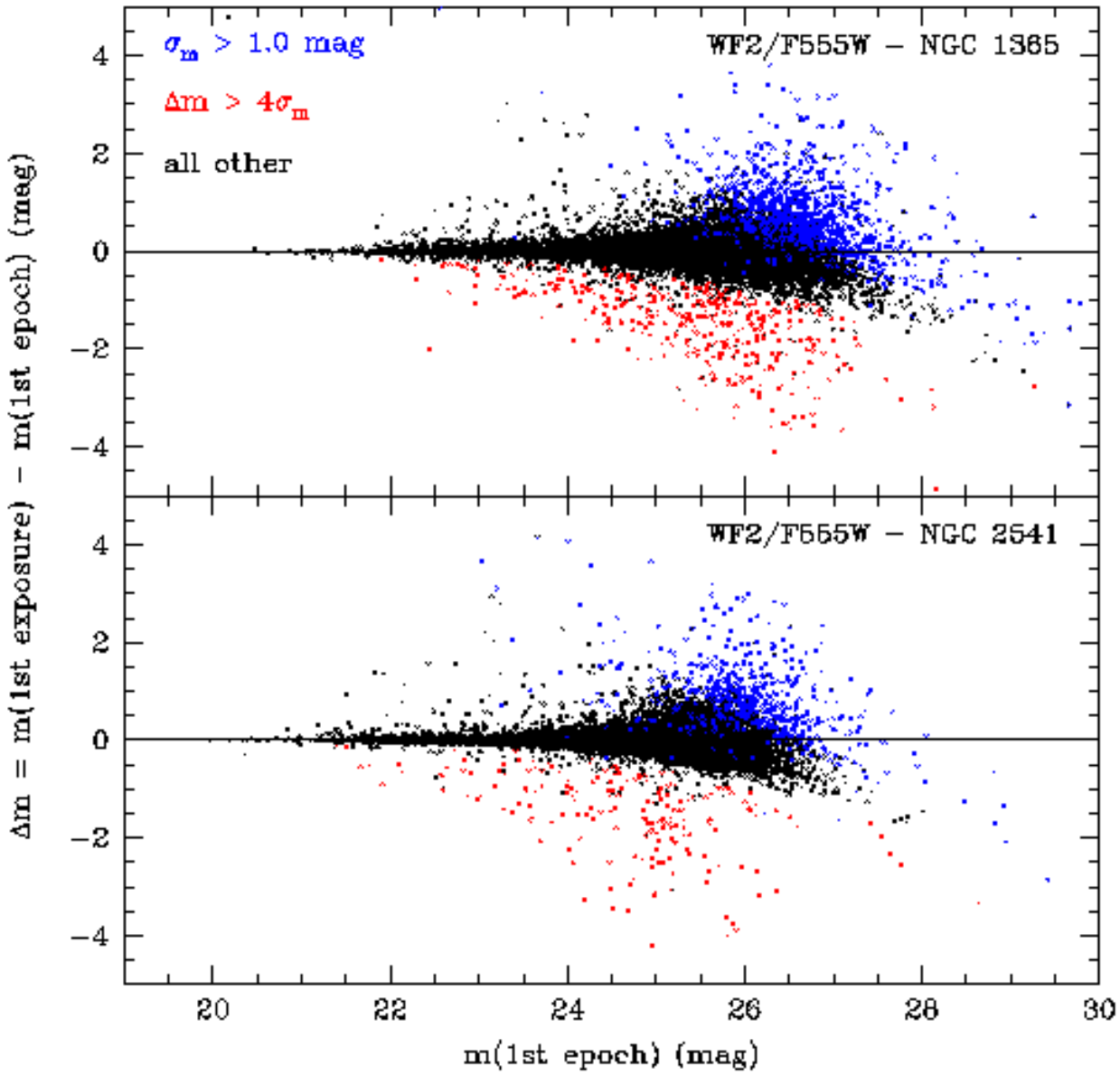

Fig. 8.— Difference between the magnitudes measured by DoPHOT for the stars in the first exposure and first epoch. Points for which this difference is larger than four times the photometric error measured in the first epoch are shown in red, points for which the photometric error is larger than 1 mag are in blue.

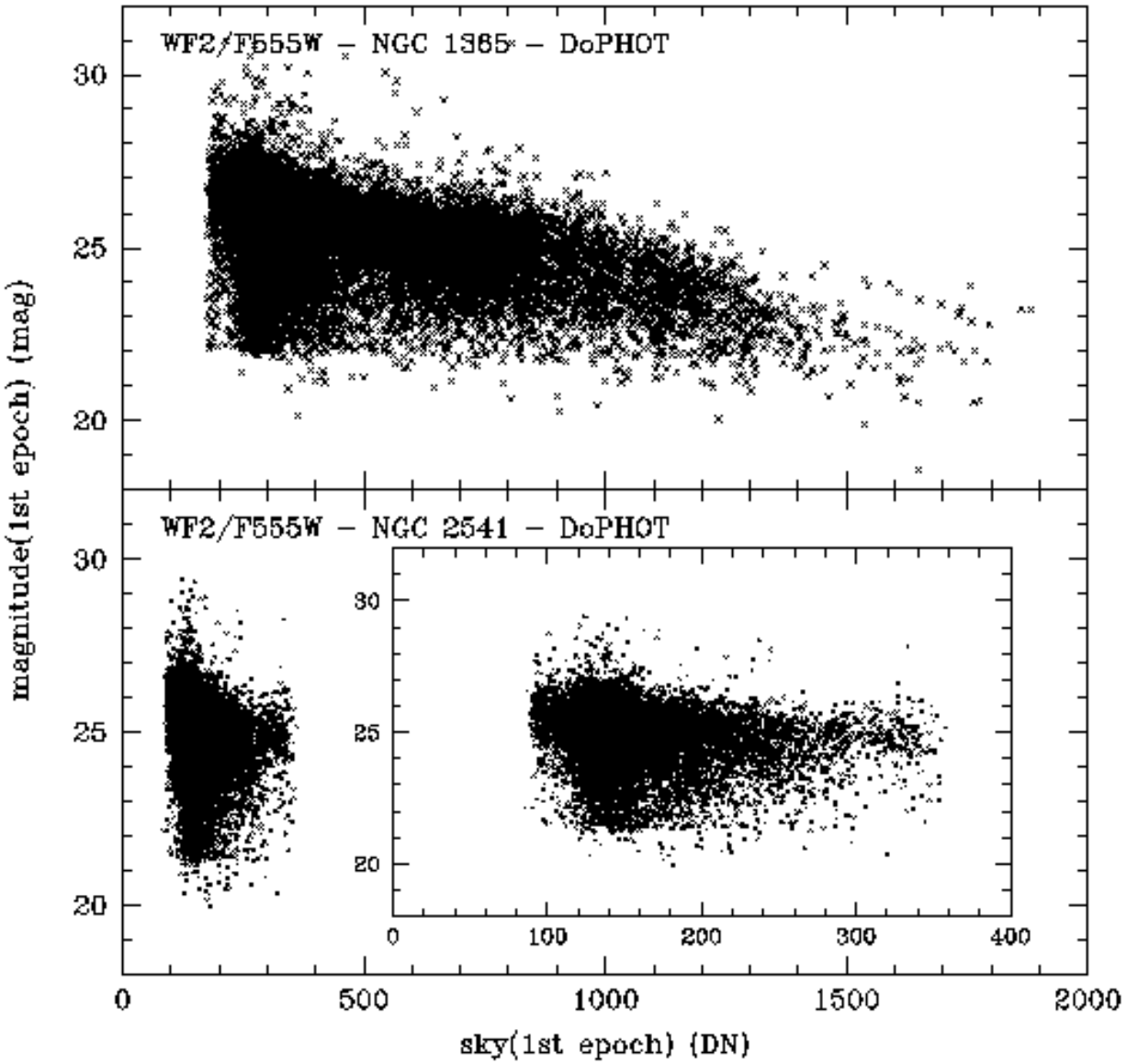

Fig. 9.— Completeness as a function of background brightness (in total number of counts) for the first epoch of NGC 2541 and NGC 1365.

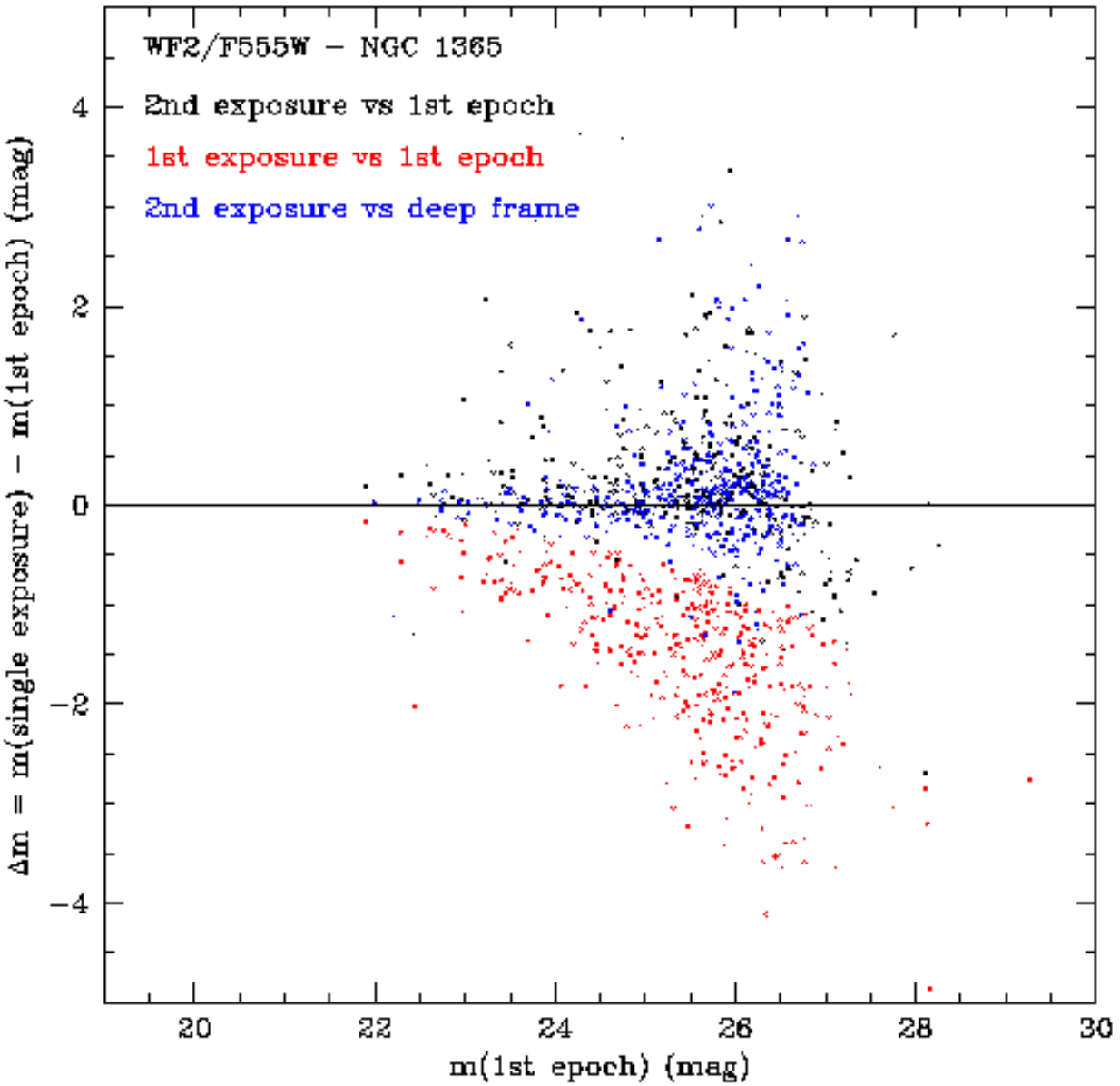

Fig. 10.— The red points are the same as in Figure 8. These stars have been singled out and their magnitude measured in the second exposure of the CR-split pair for the first epoch is compared to the one measured in the first epoch (black points) and in the deep frames (all epochs combined, blue points).

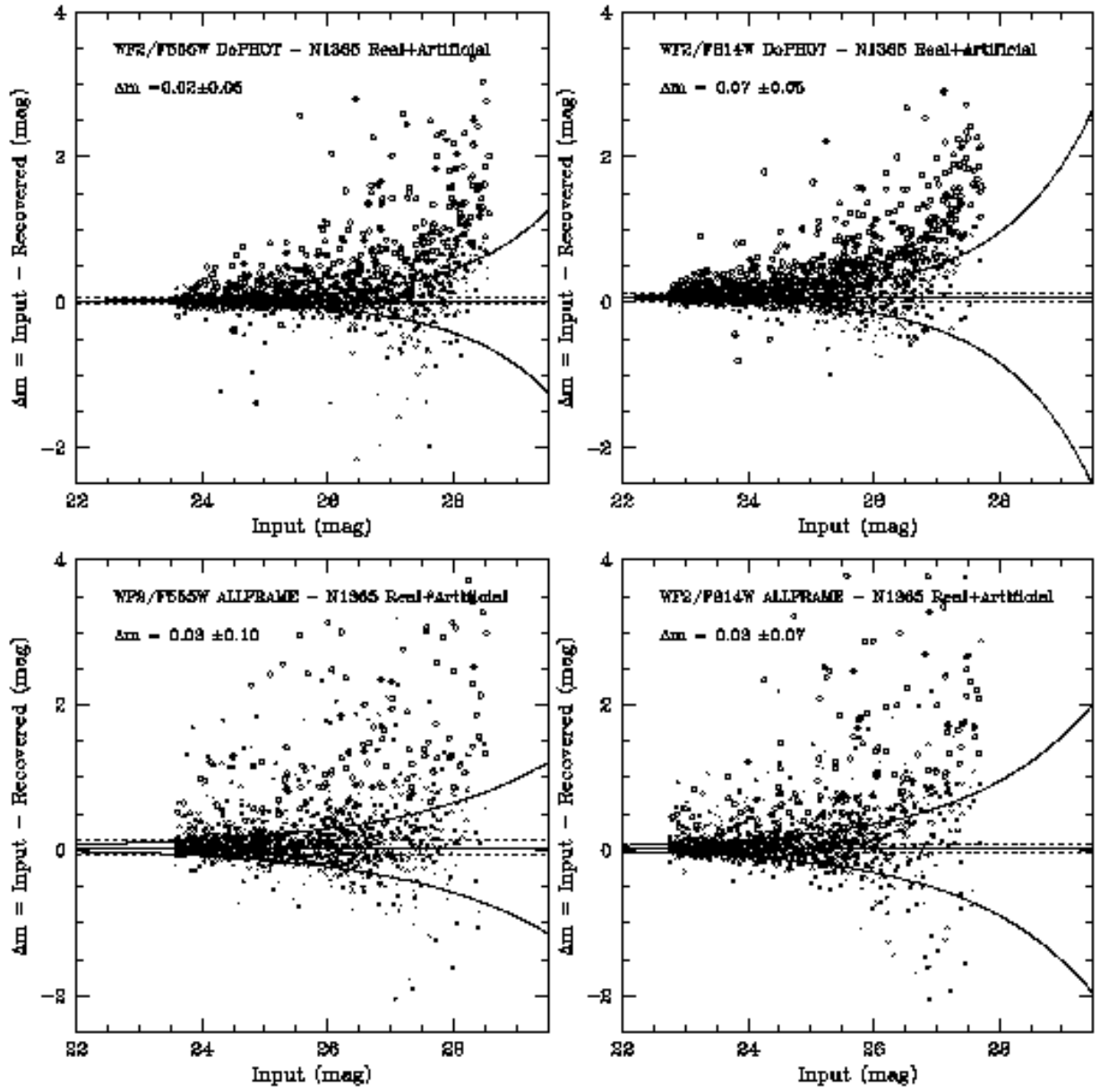

Fig. 11.— Comparison between the input magnitudes and the magnitudes derived by DoPHOT (top panels) and ALLFRAME (lower panels) from the real+artificial WF2 NGC 1365 frames. The exponential curves represent the typical error for stars whose magnitude is shown in the abscissa. Crosses corresponds to stars for which the difference is smaller than three times the measured magnitudes error σ, open circles to stars with difference $> 3\sigma$ mag.

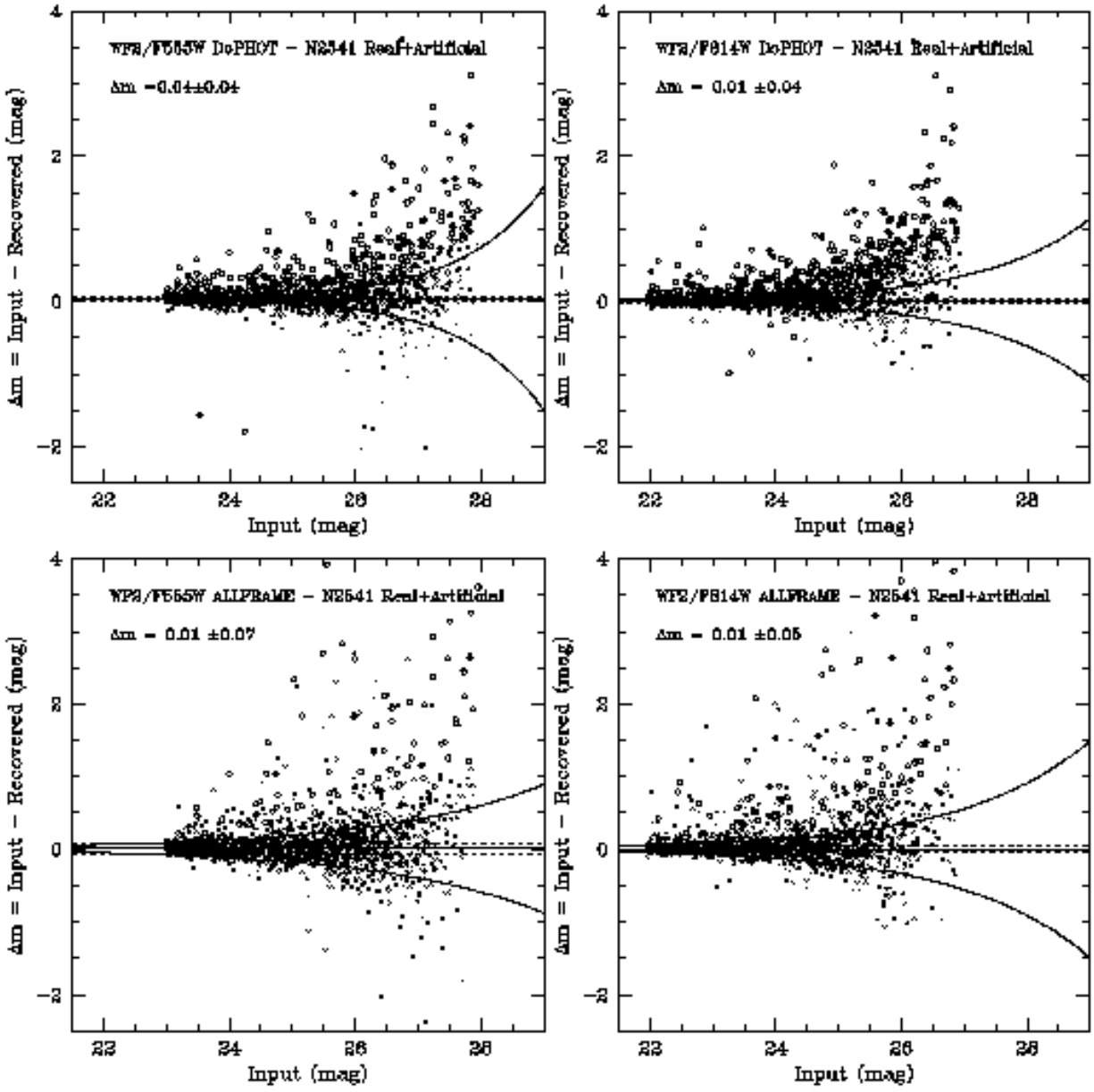

Fig. 12.— As Figure 11, but for NGC 2541.

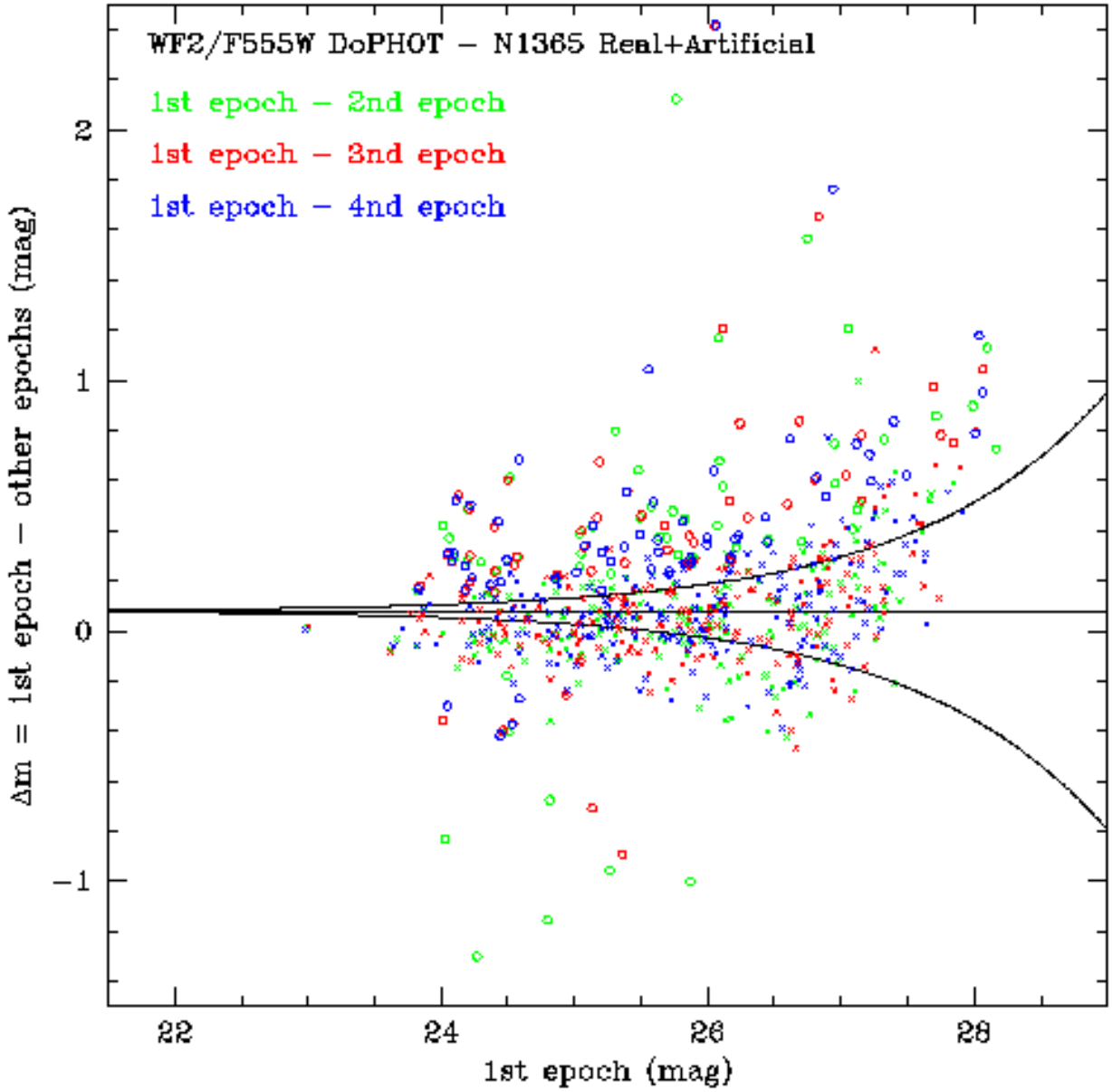

Fig. 13.— Comparison between the F814W magnitudes derived by DoPHOT for the four different epochs of the real+artificial NGC 1365 frames. The y axis plots the difference with respect to epoch 1 for epochs 2, 3 and 4, as shown by the color codes at the top of the figure. The crosses correspond to stars which are measured consistently too bright in all epochs due to confusion noise. The circles are stars which are measured too bright only in the first epoch because of a transient phenomenon, such as an unidentified cosmic ray event, but are measured correctly in all other epochs.

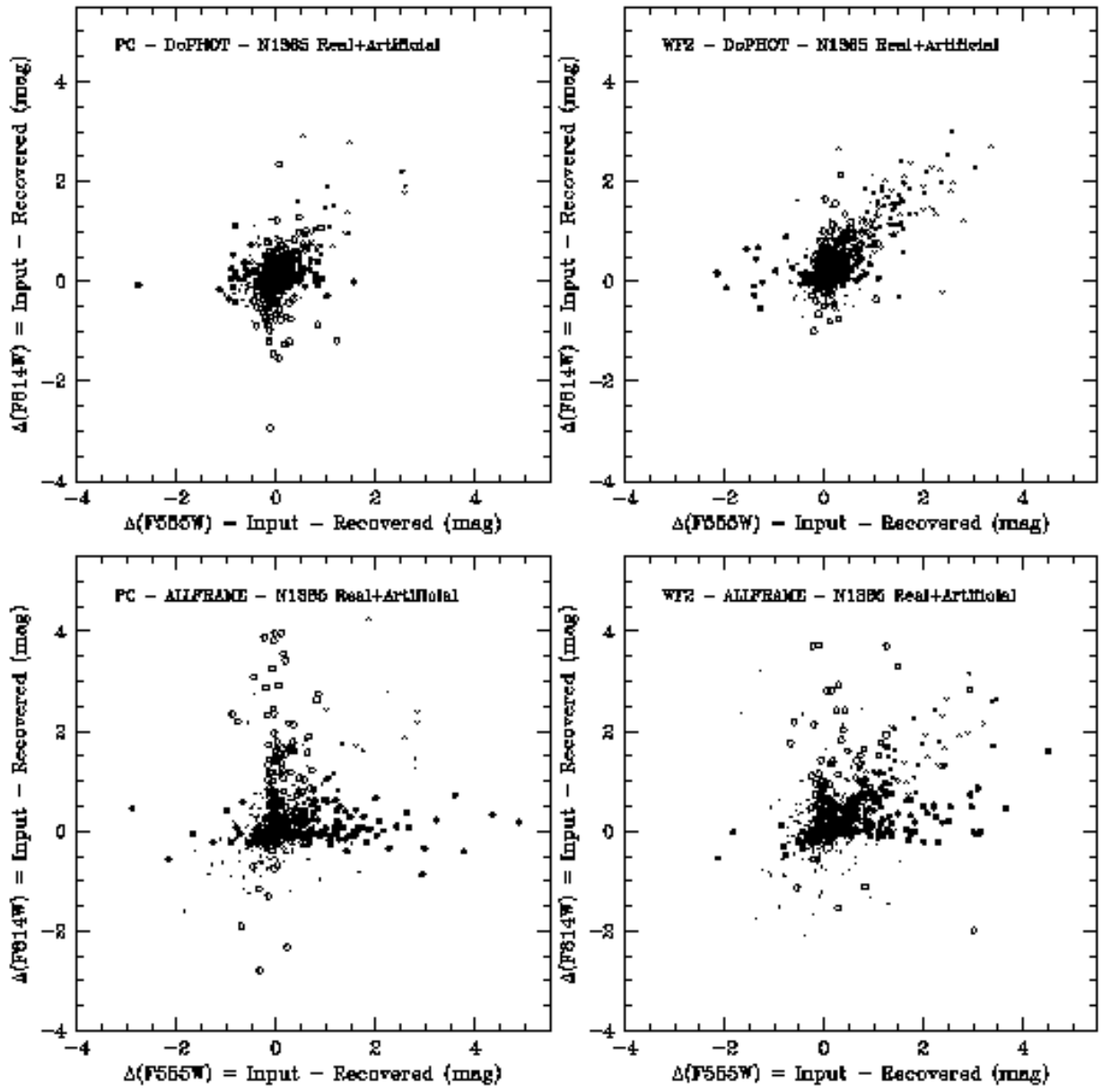

Fig. 14.— Correlation between the input and recovered magnitudes in the F555W and F814W passbands. Small points are for stars which deviate by less than three times the reported error σ in both passbands, filled and open circles are points that deviate by more than 3σ in F555W or F814W respectively, and crosses are for points deviating by more than 3σ in both passbands. Only the PC and WF2 are shown, DoPHOT photometry is plotted in the upper two panels, ALLFRAME in the lower two.

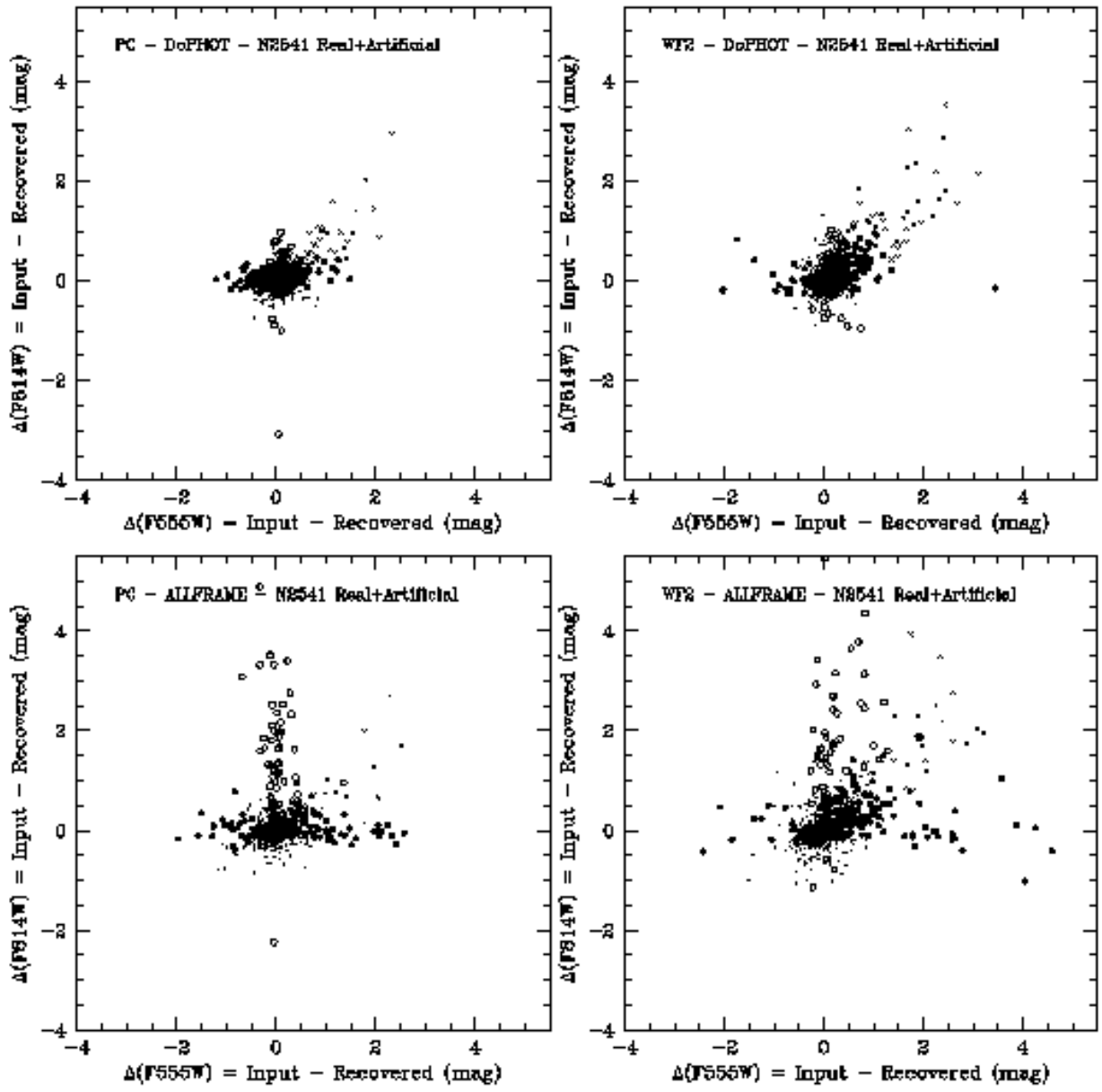

Fig. 15.— As Figure 14, but for NGC 2541.

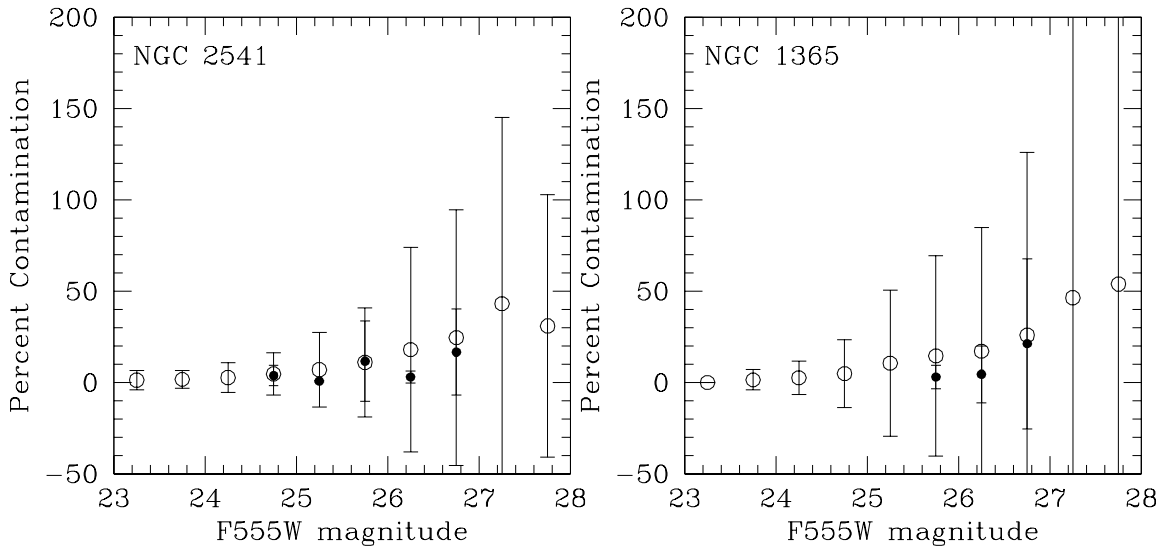

Fig. 16.— The mean and rms contamination affecting the sample of Cepheids (solid circles and smaller errorbars) and artificial stars (open circles and larger errorbars) as a function of F555W magnitudes (see text for further details).

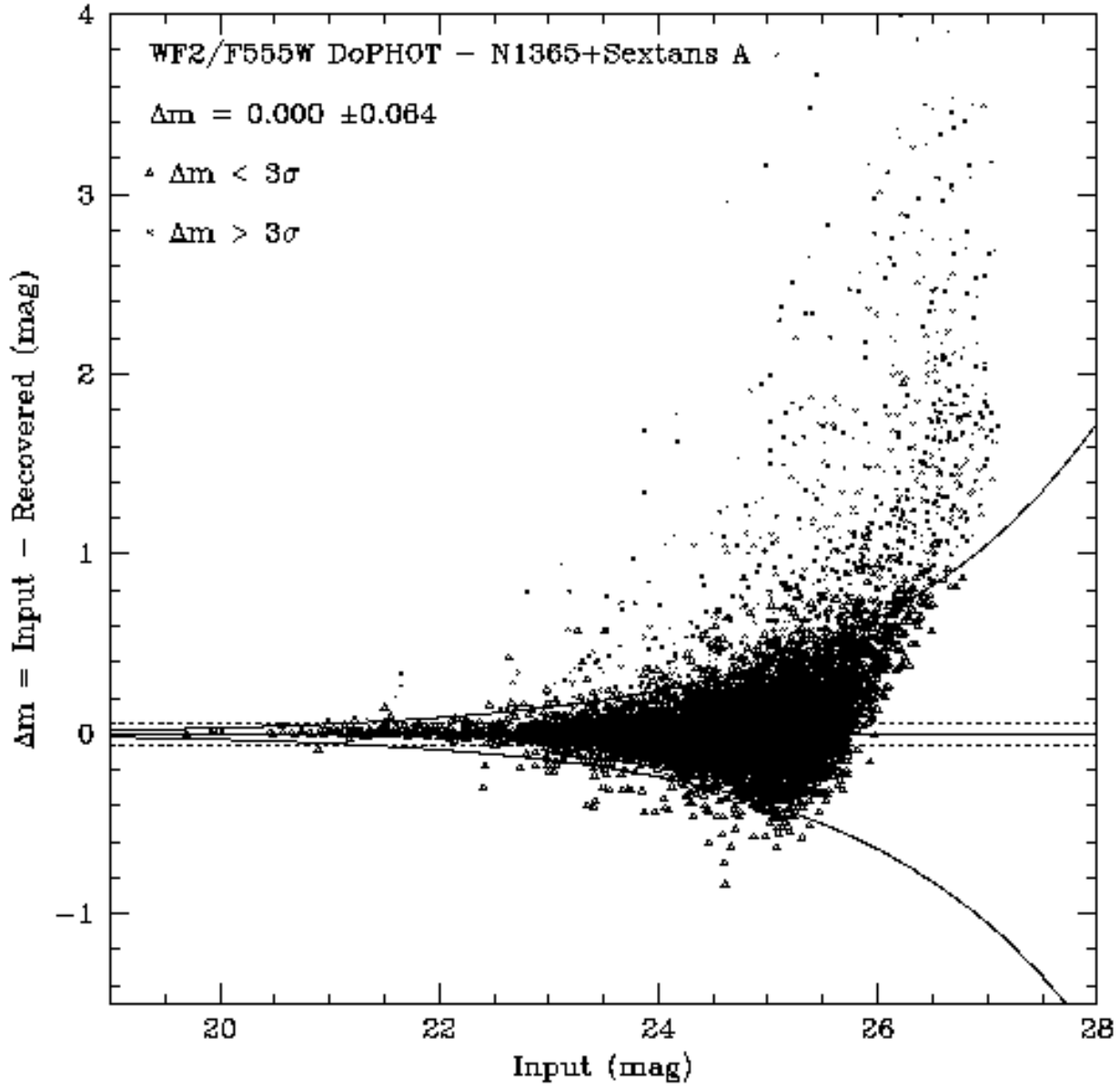

Fig. 17.— Photometric Zero point test conducted using an uncrowded Sextans A F555W/WF2 field. Input magnitudes are DoPHOT measured magnitudes in the Sextans A frame, recovered magnitudes are DoPHOT magnitudes measured when the Sextans A field is added to the F555W/WF2 first epoch of NGC 1365.

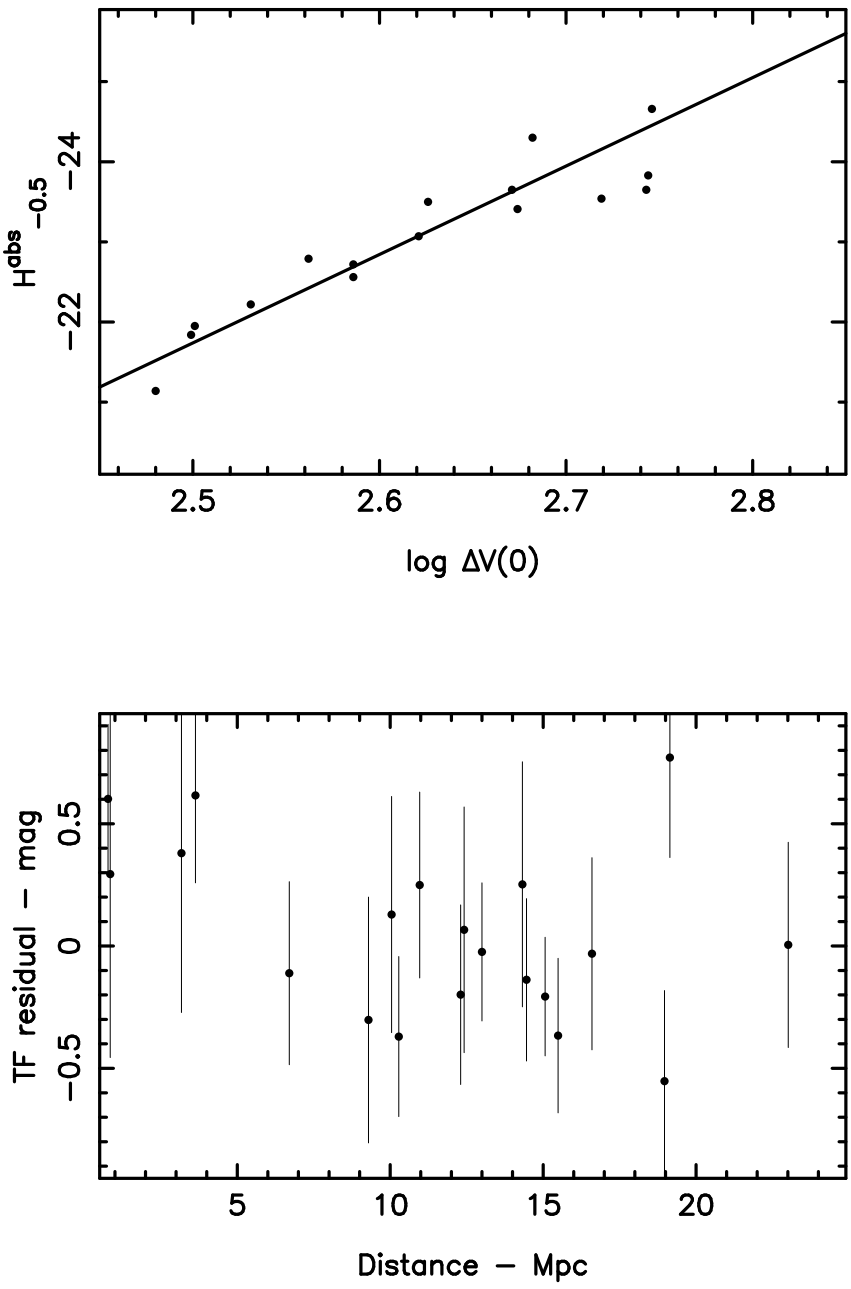

Fig. 18.— The upper panel plots the H-band Tully-Fisher relation from Sakai et al. (2000), while in the lower panel the H-band residuals are plotted against distance.


This figure "fig1_bm.gif" is available in "gif" format from:
http://arXiv.org/ps/astro-ph/9911193v1


This figure "fig2_bm.gif" is available in "gif" format from:
http://arXiv.org/ps/astro-ph/9911193v1